UNIVERSITY OF CALIFORNIA SAN DIEGO

Coordination of prefrontal-hippocampal interaction by the respiration rhythm and theta oscillations

A dissertation submitted in partial satisfaction of the
requirements for the degree Doctor of Philosophy

in

Biology

by

Sunandha Srikanth

Committee in charge:

Professor Stefan Leutgeb, Chair
Professor Jeffry S. Isaacson
Professor Jill K. Leutgeb
Professor Cory Root
Professor Bradley Voytek

2021

The Dissertation of Sunandha Srikanth is approved, and it is acceptable in quality and form for publication on microfilm and electronically.

University of California San Diego

2021

DEDICATION

To

Amma, Appa and Chachu

For their unwavering belief in my abilities

And their unconditional love.

EPIGRAPH

It's the circle of life
And it moves us all
Through despair and hope
Through faith and love
'Til we find our place
On the path unwinding
In the circle
The circle of life.

The Lion King

TABLE OF CONTENTS

LIST OF FIGURES

LIST OF TABLES

ACKNOWLEDGEMENTS

When I started my PhD in 2015, I was very naïve, to put it mildly. I thought I knew what it would be like to do research for the next 5-6 years. I thought I knew what I was getting myself into but was wholly unprepared for the months on end of no progress. I would never have been able to make it through without the support of my advisors, mentors, friends, family and well-wishers.

My advisor, Prof. Stefan Leutgeb has taught me everything I know now about performing good, rigorous research. My PhD journey has had more downs than ups, but Stefan showed me how to take it all in stride. There has not been a single meeting with him, that has not ended with the words “This is fantastic work” even after I had shown him what I considered disappointing results or if the meeting hadn’t gone well from my point of view. I have made several errors during my PhD (some more serious than others, some putting the research back several months) but never once has Stefan said a single negative word about such things. Every conversation with him has left me invigorated and filled with hope that perhaps my research was not going down the drain. His magnanimity, enthusiasm and curiosity have kept me going. Most of all, he taught me that science is, at its core, a search for the truth, something I thought I knew, but never grasped until Stefan led by example. I will forever be grateful that I chose him to be my PhD advisor.

Prof. Jill Leutgeb has been a great mentor throughout my PhD. Her probing questions made me think more deeply about my work and her keen perspective has made sure that my reasoning is devoid of major loopholes. I have also learnt from her crucial skills such as presentation skills, and how to think big picture. I am immensely grateful to

have three other amazing faculty on my dissertation committee, Prof. Brad Voytek, Prof. Cory Root and Prof. Jeffrey Isaacson who have given me invaluable advice over the years. Mine has been the most supportive committee I could have asked for. Their comments during my one-on-one meetings as well as their collective encouragement during my committee meetings always filled me with optimism and the strength to move forward for another year!

At this point, I must acknowledge my prior mentor, Prof Rishikesh Narayanan who was my advisor for my Bachelors thesis at the Indian Institute of Science, Bangalore, India. Rishi has been the kindest mentor I could have hoped for. I'm profoundly grateful that he took the time to write approximately 17 letters of recommendation for my graduate school applications. I would not be here at UCSD without his guidance. Rishi has been a constant throughput my PhD journey and has been an incredible sounding board for all things academic and otherwise.

My experience in the Leutgeb Lab has been enriched many-fold by the lab members. My first contact was with Ipshita Zutshi, a graduate student in the lab who set the bar very high! Although she graduated over two years ago, her (hugely positive) influence on the lab, and on me persists to date. She showed me by example what it means to be a successful graduate student and I'm grateful to have had such a wonderful role model. I'm thankful to Silvia Viana da Silva and Marta Sabariego, two rockstar post-docs in the lab who were always ready to help me with anything I needed in lab, despite their very busy schedules. I also saw them balance life and work brilliantly and with impeccable work ethics which has inspired me immensely. Maylin Fu, our lab manager has been my

one-stop-shop for all things lab-related – she seemed to always know all the experimental techniques and the location of all the lab supplies! My fellow grad students, Sia Ahmadi and Clare Quirk were great rant buddies and Sia, especially offered wonderful scientific advice. His breadth and depth of knowledge has been inspirational. Li Yuan, a post-doc and my office-mate has been a wonderful person to talk to and discuss science with.

When Dylan Le and Yudi Hu first started working with me to help with behavioral experiments, I was supposed to train them on techniques. This mentor-mentee relationship with them quickly turned the other way around. I was the one who learnt from them and by teaching them. I am forever grateful for the Yudi's experimental skills, punctuality, independence, and promptness. She often comes forth with wonderful ideas and suggestions, and my PhD is all the better for it. Thank you, Yudi!

Being in a different country from your homeland is difficult for everyone, and it was for me too. But I found a group of friends here who took over the role of my being my family. In no particular order, Sid, Mrittika, Prit, Kanika, Neeraja, Swetha, Nandu, Sourish, Mihir, Tapan, Sumitash, Lorraine, Bhanu, Raghu, Aravind and everyone else in the Dinner/Hike/Spam group, have been the ones I turn to when I'm feeling sad, happy or just hungry. I must thank Sid, for introducing me to the social circle here at San Diego and for the many fun parties! Prit has been the most darling of all my friends. He has always encouraged me to push forward and has been the best shopping partner I could ask for. Prit, our beach vacation home awaits! Kanika and Neeraja, both fellow Biology graduate students started off as my official and unofficial peer-mentors respectively but I'm so proud to call them my friends. Lorraine, my dance partner has inspired me to be a better person

after every conversation with her. Every interaction with Swetha, a neuroscience post-doc, is so inspiring because she is extremely well-read, and I strive to achieve that level of scholarship someday. I have also immensely enjoyed our dance practices and performances – combining two classical art forms provided a much-needed respite to academic work. Nandu, thank you for always looking out for me and caring for me, even (and especially) when I don't stay in touch! Sourish, my coffee and gelato buddy, has been solely responsible for the many good changes in my thinking over the years. Apart from these folks, my friends from college, Himani, and Vamsi, have been instrumental in helping me stay grounded. We might not speak for long periods of time, but when we catch up, we pick up where we left off, and I'm grateful for that.

I met Hemaa 10 years back and we've been inseparable since. She is the one I speak to every day, the one I've yelled at and cried to without preamble, the one who has been anything I need her to be in that moment. I can trust her to correct me when I'm wrong and cheer me on when I'm right. I would not have lasted a single day in graduate school without her. It has been one of the greatest honors of my life to call her my best friend.

When I first told my paternal grandmother (paati) that I was going to do a PhD, she asked me when I would get the Nobel Prize. I laughed then, but such is the conviction she has in my success, that grad school failures start to feel irrelevant. Thank you, paati for that conviction. My paternal grandfather (thatha), who we lost last year, would have been so proud to witness me getting my PhD. My late maternal grandfather (Balu thatha), was a gem of a person and from before I was born, took measures to ensure my safety and health. Words fail me as I try to explain how much I appreciate Balu thatha, how thankful I am for

the lessons he taught, how much I miss him and how much I wish he were here to see me graduate now.

Thank you to Viji aunty and Anitha aunty for teaching me values, dance and life lessons that have guided my journey throughout. I would be a much different person if not for them.

My parents-in-law have been a constant source of encouragement for as long as I've known them, especially if they knew that I had a rough day. They have supported me as they would their daughter. Their youthful personalities and zest for life have greatly motivated me.

My own parents, Amma and Appa, have not left a single stone unturned in their quest to provide the very best resources for me. I have not wanted for a single thing, small or big, in my entire life. Importantly, they gave me the freedom to pursue anything I dreamed of and jumped on board any journey I undertook and cheered me on with vigor. Such has been the privileged life that they have provided for me. To list down everything they have done for me and taught me would fill several books, so for now, Amma and Appa, I'd just like to say, thank you from the bottom of my heart for everything you do!

My brother, Chachu, has been my own personal cheerleader, believing me to be some sort of a superstar. I am no superstar, but his belief in me and my abilities has forced me to be a better version of myself, no matter the circumstances. I doubt I will ever rise up to the level of his faith in me. Despite his very busy schedule, I can count on him to be there for me and say a few words that I never knew I needed to hear. Thank you, Chachu for being the best brother I could ask for.

Last, but definitely not the least, I want to thank my husband, Vignesh. He's the best thing I've found at San Diego. From music and dance practices to marital bliss, we've come a long way. He has a perspective on matters, that is always practical and optimistic (sometimes, infuriatingly so) that it is impossible to stay stuck on a problem with him by my side. He has helped me navigate all aspects of life, especially during the pandemic, never once complaining about my late work hours or my lack of contribution to household chores. Thank you, Vignesh, for making sure I don't starve myself, for allowing me to rant to you even when you badly wanted to give me a solution and for being infectiously happy at all times! I love you glsv!

Chapter 2, in full, is material that is currently being prepared for submission for publication by Srikanth, Sunandha; Le, Dylan; Hu, Yudi; Leutgeb, Jill K.; and Leutgeb, Stefan. The dissertation author was the primary researcher of this material.

Chapter 3, in full, is material that is currently being prepared for submission for publication by Srikanth, Sunandha; Hu, Yudi; Leutgeb, Jill K.; and Leutgeb, Stefan. The dissertation author was the primary researcher of this material.

VITA

2015 Bachelor of Science (Research), Indian Institute of Science, Bangalore, India
2021 Doctor of Philosophy, University of California San Diego, USA

PUBLICATIONS

Srikanth, S and Narayanan, R (2015). Variability in State-Dependent Plasticity of Intrinsic Properties during Cell-Autonomous Self-Regulation of Calcium Homeostasis in Hippocampal Model Neurons. *eNeuro*

Quirk, CR; Zutshi, I; Srikanth S; Fu, M, L; Marciano, N, D; Wright, M, K; Parsey, D, F; Liu, S; Siretskiy, R, E; Huynh, T; Leutgeb, J, K; and Leutgeb, S. (2021). Precisely Timed Theta Oscillations are Selectively Required During the Encoding Phase of Memory. *In Press*.

Srikanth, S; Hu, Y; Leutgeb, J, K.; and Leutgeb, S. Theta oscillations in the prefrontal-hippocampal circuit are uncoupled from respiration-entrained oscillations in the olfactory bulb during an odor-cued working memory task. *In preparation*.

Srikanth, S; Hu, Y; Leutgeb, J, K.; and Leutgeb, S. Coordination of spike timing by theta oscillations within the medial prefrontal cortex and the hippocampus. *In preparation*.

FIELDS OF STUDY

Major Field: Biological Sciences

Studies in Biological Sciences, PhD
Professor Stefan Leutgeb

ABSTRACT OF THE DISSERTATION

Coordination of prefrontal-hippocampal interaction by the respiration rhythm and theta oscillations

by

Sunandha Srikanth

Doctor of Philosophy in Biology

University of California San Diego, 2021

Professor Stefan Leutgeb, Chair

Oscillations in the brain support cognitive functions by synchronizing activity of neuronal populations across large spatial scales. Oscillations therefore aid in

communication and information transfer between brain regions. Theta oscillations (6-9 Hz) are large amplitude oscillations in the rodent hippocampus that play a crucial role in facilitating working memory and sensory processing. Theta oscillations can accomplish this function through a number of ways including (1) coordinating with other oscillations in cortical and sub-cortical structures, and (2) regulating the spike timing of neurons within the hippocampus and in associated brain regions like the medial prefrontal cortex. In this dissertation, we investigated both mechanisms to shed light on the role of theta oscillations in memory and sensory processing.

In addition to the well-known role of theta oscillations in the prefrontal-hippocampal circuit, respiration-entrained oscillations in the olfactory bulb (OB) have been described in these structures. We first asked whether theta oscillations in the prefrontal-hippocampal circuit get coupled to these respiration-entrained oscillations and thus support sensory processing. We trained mice in an odor-cued working memory task and examined the coupling of theta and respiration-entrained oscillations during the different phases of the task. We found that these oscillations remain uncoupled to each other even when their frequencies match each other and during task phases when communication between these brain regions might be deemed necessary.

Having established that coherence between theta oscillations and respiration-coupled oscillations are not necessary for performance in an odor-cued working memory task, we then probed deeper into the role of precise timing of theta oscillations in controlling spike timing within the medial prefrontal cortex (mPFC) during a delayed spatial alternation task. We employed an optogenetic strategy to manipulate the frequency

of theta oscillations within the prefrontal-hippocampal network and assessed the effect of these manipulations on mPFC neuronal firing. A subset of the mPFC neurons responded to the artificially paced oscillations by shifting the frequency of their rhythmicity to match the stimulation frequency, specifically during the encoding and maintenance phases of the task. These results suggested that theta oscillations play a crucial role in mediating prefrontal-hippocampal interactions during encoding and maintenance of working memory.

I.

INTRODUCTION

Since the dawn of time, humans have been curious about the brain and have sought to understand what makes us, us. Thus, began the field of psychology to answer the "what", "how", and "why" of consciousness. In search of answers to these questions, researchers in the 1800s began studying the contents and structure and function of the mind, and instituted several schools of thought that dealt with various aspects of attention, consciousness and human experience (S Karakaş & E Başar, 2006).

Until the late 19th century, the human brain was thought to be an unexcitable tissue. However, seminal work by Fritch and Hitzig (Fritsch & Hitzig, 1870) demonstrated that the brain is indeed excitable and responds to electrical stimulation. At the time, the excitability and electrical responsiveness of the brain was thought to be a conduit for brain function. Donald Hebb laid down theoretical formulations on how the electrical activity in the brain could be the basis for every cognitive process that makes up the human experience (Hebb, 1949).

> *When an axon of cell A is near enough to excite cell B and repeatedly or persistently takes part in firing it, some growth process or metabolic change takes place in one or both cells such that A's efficiency, as one of the cells firing B, is increased.*

This hypothesis that came to be commonly known as the adage "Cells that fire together, wire together" became the basis for network brain activity, functional connectivity and

eventually, oscillatory electrical activity in the brain. While, evidence for electrical activity in the brain existed, the first recordings of human brain electroencephalogram (EEG) were performed by Hans Berger in 1929 (Berger, 1929). In his seminal paper, he wrote

> *The electroencephalogram represents a continuous curve with continuous oscillations in which... one can distinguish larger first order waves with an average duration of 90 milliseconds and smaller second order waves of an average duration of 35 milliseconds.*

In his paper, Berger observed the presence of spontaneous alpha waves recorded under the eyes-closed condition and beta waves during the eyes-open condition. At the time, Berger studied these oscillations as a means of understanding telepathy and so his research did not muster the interests of neuroscientists. Shortly thereafter, his research was corroborated by Adrian and Matthews (Adrian & Matthews, 1934) who formally described EEG alpha and beta oscillations in the human brain. Soon, gamma oscillations were discovered in the hedgehog mucosa in response to odor presentation (Adrian, 1942). Ironically, brain oscillations were quickly dismissed as "noise" and were believed to denote "idling" of the brain.

It wasn't until the 1980s that a paradigm shift occurred in the field of oscillatory brain dynamics. A surge in research papers studying the oscillatory dynamics in response to sensory stimuli were published, including studies that recorded from *in vitro* and *in vivo* brain tissue in animal models (for review, see (S. Karakaş & E. Başar, 2006). Brain oscillations therefore became a prime candidate by which to study and understand cognitive processes.

Hippocampus – role in memory and spatial navigation

The hippocampus is a brain region that resembles a sea horse, found in the medial temporal lobe in mammals. The sub-structures of the hippocampus named CA1, CA2, CA3, and dentate gyrus (DG) together form the hippocampus. There are two pathways through which information flows into the CA1 region of the hippocampus. In the direct pathway, afferents from entorhinal cortex (EC) layer 3 directly impinge on the CA1 neurons. In the indirect pathway, also called the tri-synaptic circuit, axonal arbors from EC layer 2 form synapses on the dendrites of DG neurons, the DG projects to CA3 neurons, and finally CA3 projects to CA1 pyramidal neurons via Schaffer Collaterals. In addition, EC sends information directly to CA2, which in turn sends it to CA1, which feeds it back to the EC. The hippocampus' role in encoding memory first became apparent in 1957 when Henry Molaison (HM) had a bilateral medial temporal lobe resection in hopes of lessening his seizures. In a seminal paper (Scoville & Milner, 1957) it was reported that although his seizures had decreased considerably following surgery, HM suffered from severe anterograde amnesia (inability to create new memories after the surgery) and partial retrograde amnesia (inability to recall information that was experienced for some time before the surgery) after the operation.

The hippocampus plays an important role not just in memory and learning, but also in spatial coding. This was established by a landmark study (O'Keefe & Dostrovsky, 1971) where single neuron activity was recorded in the hippocampus of a freely moving rat. It was observed that these hippocampal cells fired action potentials only when the rat was exploring a particular part of the arena, almost as if each hippocampal neuron (rightly

named “place cell”) was coding for a particular location in the arena (O'Keefe, 1979). Discovery of these place cells provided the basis for formation of spatial cognitive maps which might help in spatial navigation. With this path-breaking discovery, the field exploded with several studies exploring the role of the hippocampus in context-dependent memory. For example, it was shown that bilateral hippocampal lesions in rats affected performance in spatial memory tasks (Morris et al., 1982) corroborating the function of the hippocampus as a crucial brain region for spatial coding and learning and memory.

Oscillations in the rodent hippocampus

An electrode placed in the hippocampus would record electrical activity in the frequency range of 1 to 200 Hz that vary depending on the various sensory, motor and attentional processes that the animal is involved in. These electrical activity patterns or electroencephalogram (EEG) are due to synchronous firing of several disparate neuron types. The EEG of hippocampus can be classified into 4 rhythmical (theta: 4-12 Hz; beta: 12-30 Hz; gamma: 30-100 Hz; ripples: 120-200 Hz) and 2 non-rhythmical types of activity (large and small irregular amplitude activity, LIA and SIA). Each of these types of electrical activity has distinct behavioral correlates (Kramis et al., 1975; Vanderwolf, 1969). For example, the theta rhythms in the rat hippocampus are correlated to “translational movements” of the head with respect to the environment including walking, running, swimming, jumping and exploring. Theta rhythms are also prominent during rapid eye movement (REM) sleep. Gamma waves have been associated with a wide variety of odors, attention and memory encoding and beta waves with odors of predators. On the

other hand, LIA and SIA occur during slow wave sleep (SWS) and also during non-exploratory behavior including sitting quietly, eating, drinking and grooming. Large sharp waves accompany LIA activity in the CA1 region of the hippocampus during SWS and quiet sitting (Buzsáki & Draguhn, 2004). Sharp waves are believed to originate from the CA3 region of the hippocampus. Specifically, sharp wave recordings in CA1 are the aggregates of the excitatory post-synaptic potentials (EPSPs) of the Schaffer collaterals that result from synchronous firing of the CA3 pyramidal cells and last for around 50-100 ms. In addition to sharp waves, high frequency ripples (120-200 Hz) are observed during the negative peak of the sharp waves. Sharp wave ripples are observed at a frequency of 1-3Hz during SWS. Thus, each type of activity recorded from the hippocampus has a behavioral correlate (Headley & Paré, 2017).

Theta oscillations in the hippocampus

Theta oscillations (4-12 Hz) in the hippocampus occur during periods of movement, REM sleep, and alert immobility. These oscillations have been extensively studied in the context of spatial navigation. Theta oscillations have been reported to play an important role in learning and memory. Disrupting hippocampal theta oscillations severely impairs performance in hippocampal-dependent spatial memory tasks such as the delayed spatial alternation task, the radial maze, and the Morris water maze (Mizumori et al., 1990; Wang et al., 2015; Winson, 1978). Theta oscillations in the hippocampus have also been hypothesized to integrate sensorimotor information.

Although oscillations in the 4-12 Hz bands are broadly referred to as theta, it is well established that theta oscillations are of at least two types – type I (7-12 Hz) and type II (4-7 Hz). Type I theta is atropine-insensitive and is movement-related (Kramis et al., 1975; Vanderwolf, 1969). Power and frequency of type I theta oscillations increase with higher running speeds (Feder & Ranck, 1973; Kuo et al., 2011). On the other hand, type II theta is atropine sensitive, and is unrelated to movement (Kramis et al., 1975; Vanderwolf, 1969). Type II theta is elicited when the animal is exposed to arousing, vigilant and aversive conditions, such as a predator's smell, for instance (Sainsbury et al., 1987). The role of sensory processing has been attributed to theta I since higher speeds of the animal would involve more sensory information flow into the hippocampus, which could be dealt with by higher frequencies of theta I at higher speeds (Vanderwolf, 1969). However, theta II has also been hypothesized to be more involved with sensory processing since theta II increases in power when the strength of the sensory stimulus increased (Bland, 1986; Dudar et al., 1979). Type I Theta in the dorsal hippocampus has been widely thought to be paced by GABAergic neurons in the medial septum (MS), the inactivation of which causes a substantial reduction in theta power in dHpC (Brandon et al., 2011; Koenig et al., 2011; Winson, 1978).

Generation of theta oscillations in the medial septum

Theta in the dHpC has been widely thought to be paced by the medial septum (MS), the inactivation of which causes a substantial reduction in theta power in dHpC (Brandon et al., 2011; Koenig et al., 2011). However, there is conflicting evidence as to the type of

medial septal projections that are responsible for pacing theta in the HpC. The medial septum has mainly cholinergic and GABAergic innervations to the hippocampus. This has been corroborated by studies that show the cholinergic nature of theta I and theta II. Movement related theta I is dependent on GABAergic and cholinergic projections from the medial septum as well as glutamatergic projections from the entorhinal cortex (Yoder & Pang, 2005). On the other hand, both GABAergic and cholinergic projections from the medial septum are necessary for theta II (Yoder & Pang, 2005). But recent studies have shown that stimulation of glutamatergic cells in the medial septum can also induce movement-related theta I in the hippocampus, claiming cholinergic independence of theta I (Fuhrmann et al., 2015). In addition, optogenetic activation of the GABAergic septo-hippocampal pathway increases theta II whereas inhibition of the same causes a decrease in theta II (Gangadharan et al., 2016).

Oscillations in the olfactory bulb

LFP in the olfactory bulb (OB) falls into three frequency bands – theta, beta and gamma. First, the theta band (3-12 Hz) closely follows the respiratory frequency (Rojas-Líbano et al., 2014) at all respiration frequencies. Mitral/tufted cells in the OB are entrained to the respiration rhythm at low frequencies (up to 6 Hz) and fire tonically at higher respiratory frequencies (6-12 Hz) (Kay & Laurent, 1999). Beta oscillations are observed in the OB during odor presentation (Kay & Beshel, 2010; Kay & Freeman, 1998), odor-guided movement initiation (Hermer-Vazquez et al., 2007) and conditioned odor aversion (Chapuis et al., 2009). Beta oscillations (18-30 Hz) are coherent between OB and dHpC

and between OB and vHpC (Martin et al., 2007) during certain tasks. Gamma oscillations (30-100 Hz) are odor evoked and appear at the end of inhalation and during the transition to exhalation (Beshel et al., 2007; Rojas-Líbano & Kay, 2008).

Coupling between the respiration and oscillations in other brain regions

While it has been proposed that communications between the sensory cortices and the hippocampus are correlated with acquisition and retrieval memory (Buzsáki, 1996), the exact nature of these interactions is not known. Oscillations can provide a way to study these interactions since they are thought to synchronize spatially distinct networks.

Beta oscillations in the hippocampus have found to be coherent with beta oscillations in the olfactory bulb during odor discrimination tasks (Martin et al., 2007). This coherence is driven in the direction from the olfactory bulb to the dorsal and ventral hippocampal regions according to directional coherence measures (Gourévitch et al., 2010). Moreover, beta oscillations in the hippocampus disappear when the olfactory bulb is inactivated (Martin et al., 2006) and hence are proposed to be involved in odor memory processing (Martin et al., 2004).

Coherence between the olfactory bulb and the dorsal and ventral hippocampal regions has also been observed in the theta band. Theta band coherence is a measure of the coupling between hippocampal theta and the sniffing/respiration rhythm since olfactory theta is representative of the sniffing rhythm. The respiration rhythm and the hippocampal theta rhythm are coherent during odor learning and discrimination tasks (Kay, 2005;

Macrides et al., 1982). Coherence between sniffing and the hippocampal theta can be in both the forward and backward directions (Kay & Lazzara, 2010).

A respiration-related rhythm has also been observed in the piriform cortex (Fontanini et al., 2003), the dentate gyrus (Yanovsky et al., 2014), and the medial prefrontal cortex (Biskamp et al., 2017). Particularly, putative pyramidal cells and GABAergic interneurons in the medial prefrontal cortex (mPFC) are entrained to respiration, and LFP in this region is synchronized to the respiration rhythm as well. This coupling contributes to information processing in the mPFC (Biskamp et al., 2017). These studies suggest that the olfactory respiration rhythm may couple to theta band rhythms in the limbic-cortical network and contribute to sensory processing.

The medial prefrontal cortex

Previous research has established that communication between the HpC and the mPFC is crucial for working memory and long-term memory (Axmacher et al., 2008; Fuster, 2009). Ventral hippocampal inputs, rather than dorsal hippocampal inputs form the main pathway for communication between the HpC and the mPFC (Adhikari et al., 2010, 2011; Ciocchi et al., 2015; Hoover & Vertes, 2007). Specifically, the coordination of activity between the mPFC and the HpC has been shown to be imperative for spatial working memory in rodents (Backus et al., 2016; Benchenane et al., 2010; Colgin, 2011; Hyman et al., 2010; Hyman et al., 2005; Jones & Wilson, 2005; O'Neill et al., 2013; Siapas et al., 2005; Spellman et al., 2015; Zielinski et al., 2019). Two substrates for this coordination have been proposed – mPFC neuronal phase locking with HpC theta

oscillations (Adhikari et al., 2011; Hyman et al., 2005; Jones & Wilson, 2005; Siapas et al., 2005; Zielinski et al., 2019) and theta band coherence between the HpC and mPFC (Backus et al., 2016; Benchenane et al., 2010; Jones & Wilson, 2005).

In addition to being coordinated by theta oscillations, neuronal populations within the mPFC are also phase locked to other oscillations within the mouse brain. A significant body of evidence points to the coordination of mPFC-HpC interactions by a 4 Hz rhythm mediated by the ventral tegmental area (VTA) (Fujisawa & Buzsáki, 2011). mPFC neurons also get phase locked to the respiration rhythm in the OB, as mentioned previously (Biskamp et al., 2017; Moberly et al., 2018; Tort et al., 2018). It is possible that mPFC-HpC communication is dynamically modulated by multiple oscillations within the mouse brain.

Preview of the dissertation

In chapter II, the oscillatory coupling of slow oscillations in the mouse brain is probed. Movement-related theta oscillations (6-10 Hz) are generated in the septo-hippocampal network. They are thought to synchronize activity in the prefrontal-hippocampal network and mediate cognitive functions such as working memory (WM) and spatial navigation. On the other hand, sensory-evoked theta oscillations in the hippocampus are unrelated to movement and are elicited when the animal is exposed to arousing sensory stimuli. Recently, respiration related oscillations (RROs) have been reported to propagate to several neocortical and subcortical areas including the prefrontal cortex and the hippocampus. We asked whether RROs in the limbic circuit couple to canonical theta

oscillations during an odor-cued working memory task, and thus potentially integrate sensory processing with working memory retention. We found that RROs were coherent with the OB oscillations, except when RROs and theta (movement-related and sensory evoked) overlapped in frequency, suggesting that neither type of theta becomes coupled to RROs, even at matching frequencies. Therefore, OB oscillations – although observed at limbic regions do not appear to become coupled to theta oscillations, even when sensory-evoked theta is generated during odor sampling. These results suggest that entrainment of prefrontal-hippocampal oscillations to sensory-coupled oscillations is not necessary for WM, and that oscillations that are intrinsically paced rather than by sensory inputs are central to information processing by prefrontal-hippocampal circuits.

Then, in Chapter III, the role of theta oscillations in working memory is examined. Specifically, the functional significance of the precise timing of theta oscillations in mediating information processing in the prefrontal-hippocampal circuit is explored. Neurons in the medial prefrontal cortex (mPFC) have been shown to be phase locked to hippocampal theta oscillations. This phase locking, along with coherence of theta oscillations between the two regions, has been proposed to be the substrate for working memory in rodents. In chapter III, this hypothesis is thoroughly tested. Since theta oscillations have been established to be generated by anatomically isolated pacemaker cells in the medial septal area (MSA), an optogenetic approach was employed to gain control of the frequency of hippocampal theta oscillations without radically altering the firing rates or excitatory input to the hippocampus. This strategy provided us an advantage to effectively assess the importance of the precise timing of theta oscillations in coordinating

the spike timing of neurons within the mPFC. We therefore paced theta oscillations at three frequencies which were above (12 Hz), below (4 Hz) and within (8 Hz) the endogenous theta frequency range as the animals performed a delayed spatial alternation task. We found that a subset of mPFC neurons respond to septally paced oscillations. However, this effect was more pronounced in response to 8 Hz stimulation. Moreover, our results provide evidence of enhanced response to septal stimulation in the encoding and maintenance phases of the task, rather than the retrieval phase. Taken together, our study reveals the crucial role that the precise timing of theta oscillations plays in supporting spatial working memory.

II.

THETA OSCILLATIONS IN THE PREFRONTAL-HIPPOCAMPAL CIRCUIT ARE UNCOUPLED FROM RESPIRATION-ENTRAINED OSCILLATIONS IN THE OLFACTORY BULB DURING AN ODOR-CUED WORKING MEMORY TASK

Abstract

Nasal respiration results in a corresponding low frequency oscillation in the olfactory bulb (OB) from where the respiratory-related oscillations (RROs) are propagated to several brain areas including the prefrontal cortex and the hippocampus. We asked whether RROs that are propagated to these regions can be coupled to local theta oscillations in the prefrontal-hippocampal network. We used an odor-cued working memory task which included task phases in which theta oscillations in the dorsal hippocampus were observed during movement and during alert immobility. When OB oscillations differed in frequency from the theta frequency (~8 Hz), high coherence between RROs and prefrontal/hippocampal oscillations was detected at the RRO frequency. Interestingly, when OB oscillations and prefrontal/hippocampal theta frequencies overlapped coherence was substantially decreased, even during periods of odor sampling. Therefore, RROs did not become coupled to theta oscillations, including during periods when theta is elicited by sensory stimuli during immobility.

Introduction

Brain oscillations are thought to synchronize network activity and to mediate interactions across networks of cortical and sub-cortical brain regions (Buzsáki & Draguhn, 2004). For example, the hippocampal theta rhythm (4-12 Hz) is thought to integrate information between the neocortex and the hippocampus by organizing localized fast oscillations and single-unit activity within these regions. In the hippocampus, theta oscillations occur during periods of movement, but also during REM sleep and alert immobility. When occurring during alert immobility, hippocampal theta oscillations are believed to be involved in integration of sensory information. In addition to local theta oscillations in hippocampus, there is also ample evidence of theta oscillations in other brain regions. These extrahippocampal theta oscillations have been shown to be coupled to hippocampal theta. For example, neuronal populations as well as local field potentials (LFP) within the prefrontal cortex have been shown to be modulated by the hippocampal theta rhythm (Hyman et al., 2005; Jones & Wilson, 2005; Siapas et al., 2005; Zielinski et al., 2019). The prefrontal-hippocampal oscillatory interactions in the theta range have been correlated to performance in spatial working memory tasks in rodents (Benchenane et al., 2010; Jones & Wilson, 2005; Zielinski et al., 2019).

Along with the theta oscillation that were originally described in the hippocampus and have been confirmed to be coupled to prefrontal theta, oscillations in the theta range (3-12 Hz) are also prominent in other brain regions, but the similarity in frequency does not necessarily establish a functional relationship. In the olfactory bulb, oscillations in the theta range closely follow the respiration rhythm (Rojas-Líbano et al., 2014) across all

respiration frequencies. Respiration is paced by brainstem breathing centers (Feldman et al., 2013), and the nasal airflow that is generated by breathing then activates olfactory sensory neurons in the nasal epithelium during each breathing cycle (Wu et al., 2017). This mechanism entrains local activity in the olfactory bulb (OB), and a causal role of nasal airflow for olfactory oscillation has been established by the finding that the entrainment of OB network activity is diminished when nasal airflow is restricted by means of naris occlusion or tracheal breathing (Onoda & Mori, 1980; Phillips et al., 2012).

Respiration-entrained activity of OB neurons is transmitted to downstream olfactory-associated areas such as the piriform cortex (Fontanini et al., 2003) and the barrel cortex (Ito et al., 2014) where respiration-related oscillations (RROs) have been observed. RROs have also been reported further downstream in regions of the medial prefrontal cortex (Biskamp et al., 2017) and in the hippocampus (Lockmann et al., 2016; Nguyen Chi et al., 2016; Yanovsky et al., 2014) in addition to a number of cortical and subcortical brain regions spanning the whole rodent brain (Tort et al., 2018). Moreover, RROs in the mPFC, barrel cortex and the hippocampus are disrupted in the absence of signals from the OB or disturbance of nasal airflow (Biskamp et al., 2017; Ito et al., 2014; Moberly et al., 2018; Nguyen Chi et al., 2016; Yanovsky et al., 2014) suggesting that RROs in these regions are mediated by direct or indirect projections from the OB.

Further work on RROs within the hippocampus has mostly focused on periods when RROs differ in frequency from theta oscillations during running, immobility and anesthesia (Nguyen Chi et al., 2016; Yanovsky et al., 2014). During such periods, RROs have a different depth profile than theta oscillations in the hippocampus, suggesting that

RROs are separate from and co-exist with theta oscillations in the hippocampus. Contrasting evidence comes from studies which showed that the olfactory oscillations and the hippocampal theta oscillations become coherent during periods of sniffing in odor learning and discrimination tasks (Kay, 2005; Macrides et al., 1982). These latter studies suggest that this coherence between the hippocampal and olfactory networks mediates sensorimotor integration in the hippocampus. Taken together, it is unclear whether RROs and theta oscillations are separate or coupled oscillations when they overlap in frequency. In particular, it is possible that theta oscillations get coupled to RROs when they overlap in frequency, thus serving as a conduit for memory and sensory processing in the prefrontal-hippocampal circuit.

We therefore asked whether the LFP in the prefrontal-hippocampal regions are coupled with the respiration-entrained oscillations in the olfactory bulb (OB). We recorded LFPs across brain regions with prominent oscillations in the theta range including the hippocampus and prefrontal cortex, as well as the olfactory bulb (OB). To be able to test whether the coupling may differ during periods of mobility versus during alert immobility, we used an odor-cued working memory task where oscillations in the theta range occur during running on the maze but also during immobility in the odor sampling period.

Results

To investigate the coupling between the respiration-coupled rhythm in the OB and theta oscillations in the mPFC and hippocampus, we simultaneously recorded LFP signals in these brain regions. Because dorsal (dHC) and ventral (vHC) hippocampus are

connected to different degrees to mPFC (Hoover & Vertes, 2007), we placed separate recording electrodes in the dHC and the vHC. Within mPFC, we focused on the prelimbic,

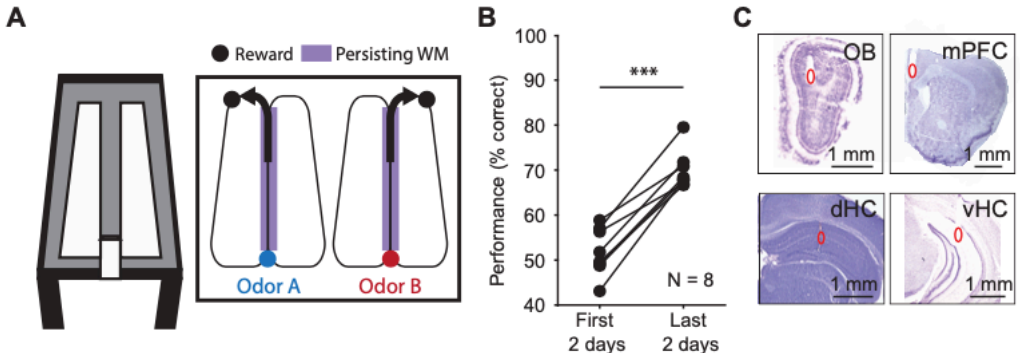

Figure 2.1 – Schematic of the task.

A. Odor-cued working memory task schematic is shown. Mice were trained to sniff one of two pseudo-randomly delivered odors at the odor port at the bottom of the stem arm and make a turn at the top of the stem arm based on the odor they sampled. Correct choices were rewarded at the reward zones. **B**. Performance during the first two days and last two days of behavioral testing (n=8 mice; Paired t-test $t(7) = 10.08$, $p<.001$) **C**. Example recording electrode locations in OB, mPFC, dHC and vHC are shown in cresyl-violet stained brain slices.

infralimbic, and anterior cingulate areas because of their direct and indirect connections with hippocampus. Respiration-entrained oscillations as well as theta oscillations have been detected in all of these regions in previous studies (Tort et al., 2018). To be able to examine oscillations across a range of behavioral states, we trained mice in an odor-cued working memory task (**Fig 2.1A**). Briefly, mice (n=8) were trained to run on a figure-8 maze in which an odor port was placed at one end of the stem arm where one of two odors (A: isoamyl acetate; B: ethyl acetate) was delivered in a pseudorandom fashion. Mice were trained to sample the odor by poking their nose into the odor port and to then run down the stem arm to make their choice to turn left or right. Correct choices were rewarded with a single chocolate sprinkle. As expected, initial performance was at chance level. Using a

criterion of 65 % correct during at least 2 of 3 days, mice learned the task within 15±5 days. Accordingly, performance during the last two days of testing (median = 70.72% correct) was better than during to the first 2 days (median = 50.69% correct) ($Z = 3.31$, $p<.001$, one-tailed Wilcoxon signed-rank test) (**Fig 2.1B**). Recording sites in the OB, mPFC, dHC and vHC were confirmed in histological material (**Fig 2.1C**). Since histological confirmation of electrode locations was not possible for one animal, we included only 7 of 8 animals for all LFP analysis. All analyses were performed on data from the last three days of recordings for each animal.

Predominant OB frequencies range from 3-12 Hz in all task phases

The task was parsed into four task phases with distinct behavioral patterns – return arm where animals ran without a memory load, stem arm where animals ran after odor sampling, odor sampling when animals actively sampled an odor, and reward arm where animals were rewarded for correct performance. Time periods when animals transitioned between these phases were not considered. The phases were grouped based on running speed. During the odor sampling period, the animals poked their noses into the odor port and sampled the odor, effectively having zero velocity during this period. Correspondingly, all analyses on the reward arm were performed only for periods with low velocity (less than 5 cm/s) so that meaningful comparisons can be made with odor sampling periods. Conversely, we confirmed that running speeds on the return arms and on the stem were high and approximately matched (**Fig 2.2A**). Although the velocity profiles ranged from immobility in the odor port to high running speeds on the return arms (**Fig 2.2A**), the

predominant frequencies of the OB power spectrum within each of the four task phases showed only minor differences and encompassed the entire range from 3 Hz to 12 Hz

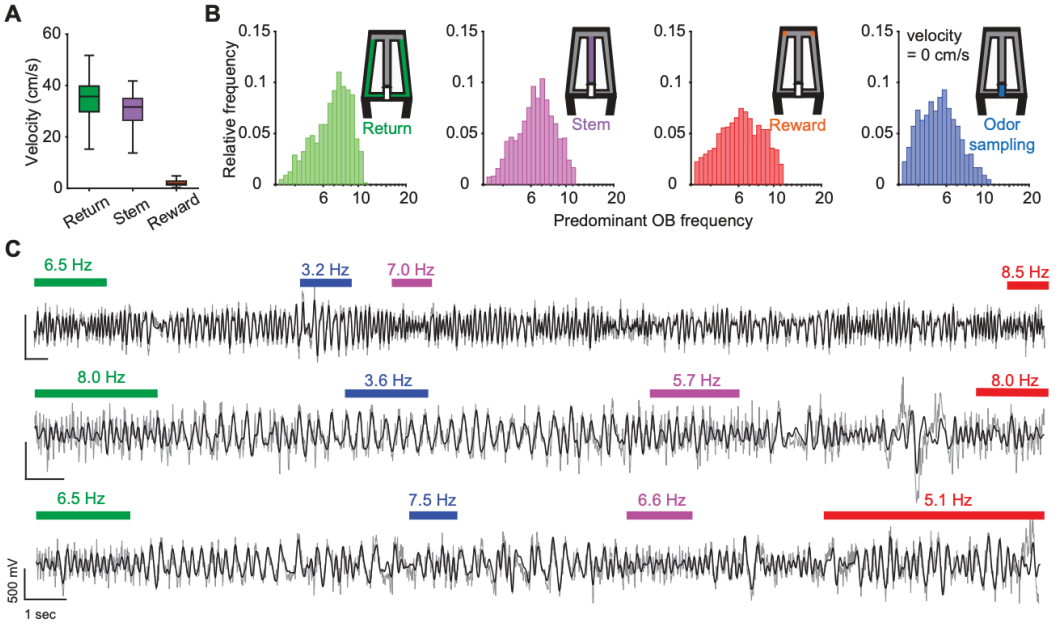

Figure 2.2 – Predominant OB frequencies range from 3-12 Hz within each task phase across trials.

A. Velocity of the animals (7 mice; 1207 trials) in each maze zone. Velocity in the odor port was zero since animals poked their noses into the odor port during the time of odor sampling. **B**. Relative frequencies of predominant OB frequency in each task phase. **C**. Example OB traces in example trials (grey: raw traces, black: filtered traces). Colored bars indicate time periods when animals were in the respective task phase (Green: Return arm, Blue: Odor sampling, Purple: Stem arm, and Red: Reward zone). Corresponding predominant OB frequency are displayed.

across trials (median±iqr in return: 7.02±2.77 Hz; stem: 6.58±2.60 Hz; reward: 6.16±3.26 Hz; odor sampling: 5.41±2.42 Hz) (**Fig 2.2B**). Moreover, within a trial, predominant OB frequencies varied across task phases (**Fig 2.2C**) with only weak correlations among them (Spearman correlation coefficient < 0.5) (**Fig 2S.2**). Because OB oscillations in this frequency range have been firmly established as being generated by respiration (Jessberger

et al., 2016; Phillips et al., 2012; Rojas-Líbano et al., 2014), we refer to these oscillations as respiratory-related oscillations (RROs).

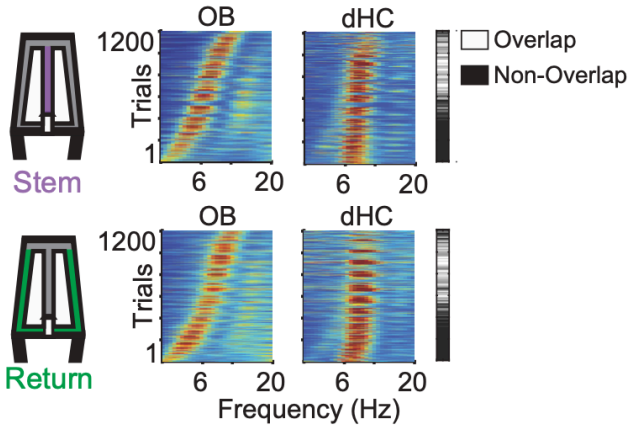

Figure 2.3 – Defining "overlap" and non-overlap" trials.

Trials were categorized as "overlap" (white) or "non-overlap" (black) depending on the predominant OB frequency and dHC theta frequency in each task phase in every trial. Categorization as "overlap" or "non-overlap" was done independently for each task phase. Trials that had a difference of <= 1Hz between the dHC theta frequency and the predominant OB frequency were categorized as "overlap".

Our task design allowed us to assess the coordination of RROs with movement-related and sensory-evoked theta oscillations in the prefrontal-hippocampal network because it included task phases when either type of theta is prominent. For example, high amplitude movement-related theta oscillations were observed on the stem and return arms (**Fig 2S.3A**). Although lower in amplitude, theta oscillations in the dHC were also detected on reward arms and during odor sampling despite the animals moving slowly or being immobile. Hippocampal theta oscillations during odor sampling periods are therefore considered sensory evoked (**Fig 2S.3B**).

Since OB predominant frequencies were distributed over the entire 3-12 Hz range while canonical dHC theta was concentrated in the 7-11 Hz range, there were trials in which

OB frequency and canonical dHC theta frequency either differed or overlapped. We therefore grouped trials into two categories – trials with overlapping dHC theta and OB frequency (<=1 Hz apart) and trial with non-overlapping dHC theta and OB frequency (>1 Hz apart) (**Fig 2.3**). Grouping of trials as "overlapping" or "non-overlapping" was done independently for each task phase within a trial. For example, a trial could be grouped as overlapping for analysis on stem arm and non-overlapping for analysis done on return arm.

RROs are observed in the prefrontal-hippocampal network in parallel with either movement-related or sensory-evoked theta oscillations

We first investigated the coordination between movement-related theta oscillations and RROs in trials with non-overlapping frequencies. Periods of running on the stem, running on return arms, and odor sampling were analyzed separately. In the stem and return arms, LFP in the prefrontal-hippocampal network showed two detectable peaks in the 3-12 Hz range – one matching the frequency of RROs and another oscillation with a frequency of ~8 Hz (canonical movement-related theta) (**Fig 2.4A, 2.4B**). Similarly, during odor sampling periods, LFP in the prefrontal-hippocampal network exhibited two oscillations in the 3-12 Hz range – one matching the frequency of RROs and another oscillation with a frequency of ~7-8 Hz (canonical sensory-evoked theta) (**Fig 2.4B**). In these trials, coherence spectra between oscillations in the prefrontal-hippocampal regions and the OB revealed high coherence at frequencies matching the predominant OB frequency, reflecting the coherence of RROs within the prefrontal-hippocampal network

even when these oscillations were not the predominant oscillations in the prefrontal-hippocampal network (**Fig 2.4B**).

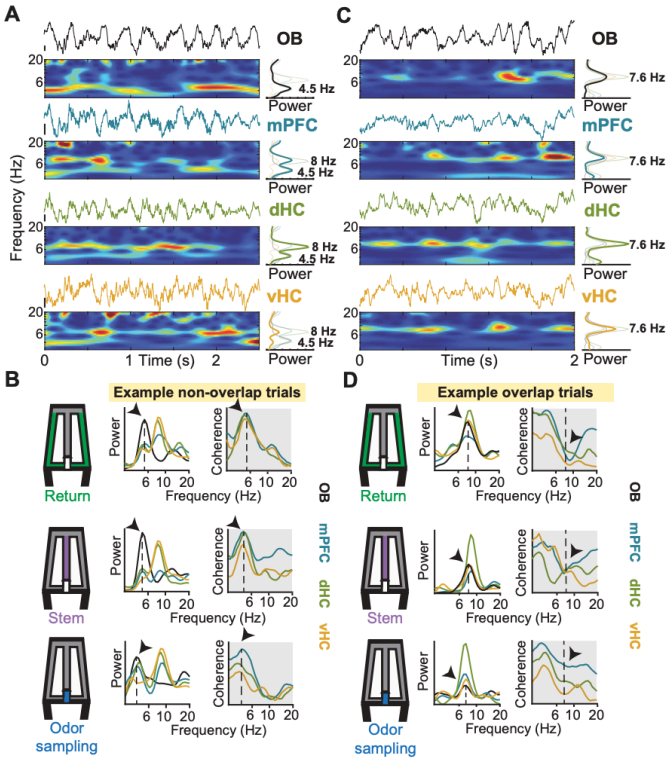

Figure 2.4 – RROs were observed in the mPFC-dHC-vHC network in parallel with movement-related or sensory-evoked theta oscillations.

A. Example raw traces and corresponding time-frequency spectrograms of simultaneously recorded LFP from the OB, mPFC, dHC and vHC are shown for a period when the animal was on the stem arm of the maze. Here, an example of theta oscillations in the mPFC-dHC-vHC regions non-overlapping in frequency with the predominant OB frequency is shown. **B**. Time averaged power spectra (left) and coherence spectra (right) are shown for three maze zones (return arm, stem arm and odor sampling period) in "non-overlap" trials. Dotted lines and arrows indicate the frequency of the predominant OB oscillation in the respective trials. OB-mPFC, OB-dHC and OB-vHC coherence is higher at the frequency matching the predominant OB frequency, compared to the theta frequency. **C**. Similar to **A** but an example of theta oscillations overlapping in frequency with the predominant OB frequency is shown. **D**. Similar to **B** but for example "overlap" trials. Dotted lines and arrows indicate the frequency of the predominant OB oscillation in the respective trials. OB-mPFC, OB-dHC and OB-vHC coherence was low at the frequency matching the predominant OB frequency, indicating that theta oscillations in the mPFC-dHC-vHC network did not couple to respiration-entrained oscillations in the OB.

Movement-related and sensory-evoked theta oscillations are uncoupled to RROs.

While it is expected that RROs and canonical theta (either movement-related or sensory-evoked) are separate oscillations when their frequencies are non-overlapping, the question remains whether RROs show coupling with either type of theta oscillation when the frequencies are matching. By selecting trials in which predominant OB frequencies and hippocampal frequencies overlapped, we obtained spectrograms in which RRO frequencies in the power spectra closely matched canonical theta oscillations of mPFC, dHC and vHC regions (**Fig 2.4C, 2.4D**). We then computed the coherence spectra between OB and prefrontal oscillations and between OB and hippocampal oscillations in trials with overlapping frequencies. If theta oscillations in the prefrontal-hippocampal network also get coupled to RROs in trials with overlapping frequencies, we would expect a high coherence for this trial type. In contrast, we found a significant decrease in coherence in trials with overlapping frequencies compared to trials with non-overlapping frequencies for all combinations between OB oscillations and cortical regions and for all maze segments (return arm: OB-mPFC: $Z=-10.79$, $p<.001$; OB-dHC: $Z=-9.09$, $p<.001$; OB-vHC: $Z=-8.54$, $p<.001$, Wilcoxon signed-rank test; stem: OB-mPFC: $Z=-7.67$, $p<.001$; OB-dHC: $Z=-4.88$, $p<.001$; OB-vHC: $Z=-4.82$, $p<.001$, Wilcoxon signed-rank test; odor sampling period: OB-mPFC: $Z=-10.09$, $p<.001$; OB-dHC: $Z=-7.34$, $p<.001$; OB-vHC: $Z=-6.61$, $p<.001$, Wilcoxon signed-rank test) (**Fig 2.4D, 2.5**). The decrease in coherence in trials with overlapping compared to non-overlapping frequency could not be explained by a difference in power of these oscillations (return arm: mPFC: $Z=10.73$, $p=1.00$; dHC: $Z=19.15$, $p=1.00$; vHC: $Z=13.59$, $p=1.00$, Wilcoxon signed-rank test; stem: mPFC:

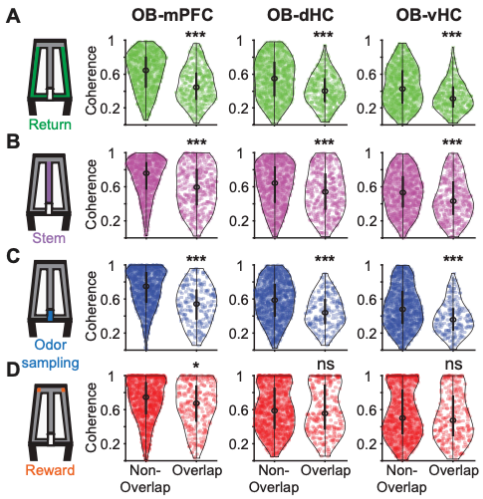

Figure 2.5 – Respiration-entrained oscillations in the OB were uncoupled to movement-related and sensory-evoked theta oscillations in the mPFC-dHC-vHC network.

Violin plots of OB-mPFC, OB-dHC, and OB-vHC coherence in the return arm (**A**), the stem arm (**B**), the odor sampling period (**C**) and the reward arm (**D**) are shown in trials with overlapping and non-overlapping theta and RRO frequencies. Coherence was calculated at the RRO frequency in each trial. A significant decrease in coherence was found in trials with overlapping RRO and theta frequencies compared to trials with non-overlapping frequencies for all prefrontal-hippocampal regions in the return arm (OB-mPFC: Z=-10.79, p<.001; OB-dHC: Z=-9.09, p<.001; OB-vHC: Z=-8.54, p<.001, Wilcoxon signed-rank test), stem arm (OB-mPFC: Z=-7.67, p<.001; OB-dHC: Z=-4.88, p<.001; OB-vHC: Z=-4.82, p<.001, Wilcoxon signed-rank test) and odor sampling period (OB-mPFC: Z=-10.09, p<.001; OB-dHC: Z=-7.34, p<.001; OB-vHC: Z=-6.61, p<.001, Wilcoxon signed-rank test). In the reward zone, only OB-mPFC coherence was decreased in trials with overlapping RRO and theta frequencies compared to trials with non-overlapping frequencies.

Z=8.58, p=1.00; dHC: Z=21.51, p=1.00; vHC: Z=14.34, p=1.00, Wilcoxon signed-rank test; odor sampling period: mPFC: Z=4.90, p=1.00; dHC: Z=14.34, p=1.00; vHC: Z=8.59, p=1.00, Wilcoxon signed-rank test). A comparison of velocities in trials with overlapping and non-overlapping frequencies did not reveal any difference (return: Z=-1.44, p=.07, stem: Z=7.21, p=1.00, Wilcoxon signed-rank test). These results suggest that canonical

types of theta oscillations in cortical regions do not couple to the respiration-entrained oscillation in the OB during periods of running when movement-related theta is generated as well as during period of odor sampling when sensory-evoked theta oscillations are generated in response to active sampling of the odor.

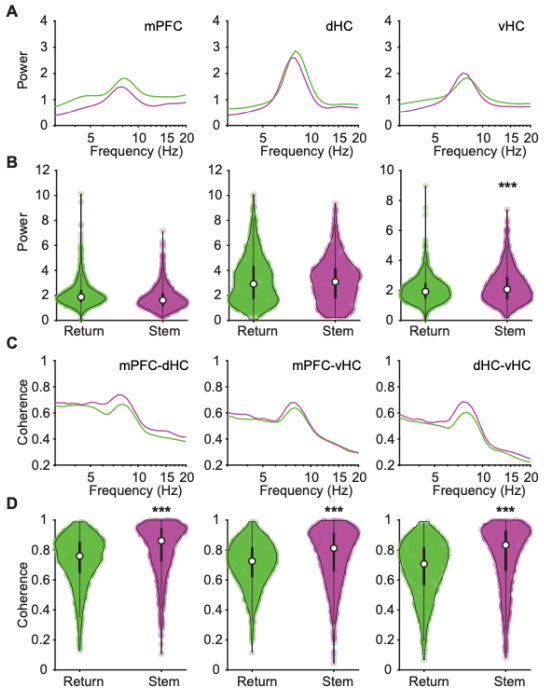

Figure 2.6 – Movement-related theta oscillations in the prefrontal-hippocampal regions were more coherent in the stem arm compared to return arm.

A. Trial averaged power spectra of mPFC, dHC and vHC regions are shown for periods on the stem (purple) and return (green) arms. **B**. Violin plots of peak movement-related theta power in the mPFC, dHC and vHC regions during periods on the stem and return arms across all trials are shown. The mPFC and dHC regions did not show an increase in movement-related theta power in the stem arm compared to the return arm (mPFC: $Z=9.78$, $p=1.00$; dHC: $Z=0.75$, $p=0.77$), but vHC theta power was higher in the stem arm compared to the return arm (vHC: $Z=-4.30$, $p<.001$, Wilcoxon signed-rank test). **C**. Trial averaged coherence spectra for pairs of regions (mPFC-dHC, mPFC-vHC and dHC-vHC) are shown. **D**. Violin plots of coherence of movement-related theta oscillations between all three pairs of regions was compared between the stem (purple) and return (green) arms. Coherence of movement-related theta oscillations was higher in the stem arm compared to the return arm (mPFC-dHC: $Z=-14.34$, $p<.001$; mPFC-vHC: $Z=-11.49$, $p<.001$; dHC-vHC: $Z=-14.64$, $p<.001$, Wilcoxon signed-rank test).

Movement-related theta oscillations in the prefrontal-hippocampal regions were more coherent in the stem compared to return arm.

After establishing that RROs do not couple to either type of theta oscillations in any of the cortical regions, we explored whether we could nonetheless identify dynamic coordination of movement-related theta oscillations between cortical areas, which has previously been described in similar tasks. We analyzed the two task phases (stem and return arms) when movement-related theta oscillations were observed (**Fig 2S.3**). While the mPFC and dHC regions did not show an increase in movement-related theta power in the stem compared to the return arms (mPFC: Z=9.78, p=1.00; dHC: Z=0.75, p=0.77), vHC theta power was higher in the stem compared to the return arms (vHC: Z=-4.30, p<.001, Wilcoxon signed-rank test) (Fig 6A). Although there was a modest increase in movement-related theta power in only the vHC, coherence of movement-related theta oscillations between all three pairs of regions was higher in the stem compared to the return arms (mPFC-dHC: Z=-14.34, p<.001; mPFC-vHC: Z=-11.49, p<.001; dHC-vHC: Z=-14.64, p<.001, Wilcoxon signed-rank test) (**Fig 2.6B**).

Even though we examined odor-guided working memory in our task, the figure-8 maze is often used to assess spatial alternation behavior in rodents, and we observed that mice's default response was to show spatial alternation before gaining proficiency in following the odor cued task. We reasoned that mice's tendency to show spatial alternation would continue to interfere with odor-guided choices even after the mice performed above chance in the odor-guided version. To test this possibility, we analyzed four different types of trials – alternating correct, alternating incorrect, non-alternating correct, non-alternating

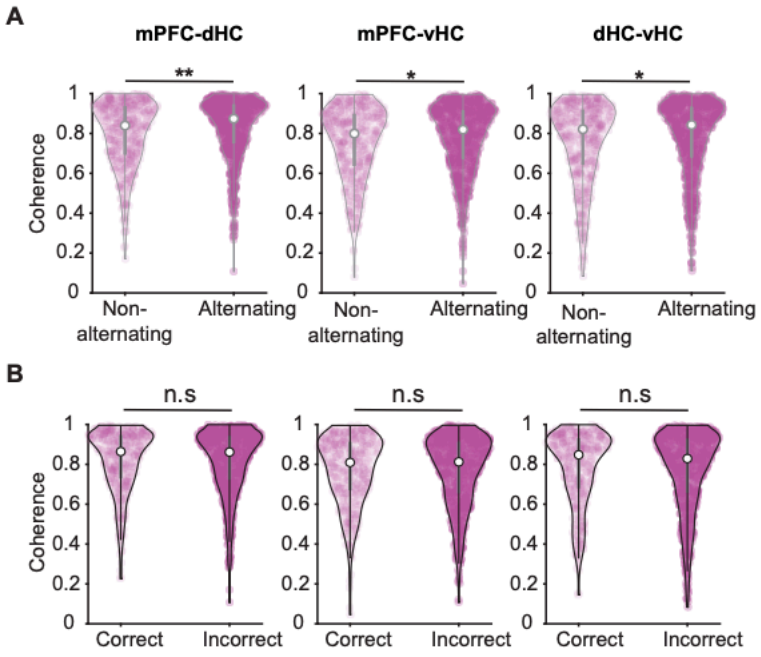

Figure 2.7 – Movement-related theta oscillations in the stem arm are more coherent in alternating trials compared to non-alternating trials.

A. Coherence of movement-related theta oscillations between pairs of regions in the mPFC-dHC-vHC network in the stem arm is shown for alternating trials and non-alternating trials. Coherence was significantly higher during alternating compared to non-alternating trials (mPFC-dHC: $Z=2.80$, $p<.01$; mPFC-vHC: $Z=2.37$, $p<.05$; dHC-vHC: $Z=2.40$, $p<.05$, Wilcoxon signed-rank test). **B**. Same as **A**, but for correct and incorrect trials. Coherence was not different between correct and incorrect trials (mPFC-dHC: $Z=-0.48$, $p=0.63$; mPFC-vHC: $Z=-0.05$, $p=0.96$; dHC-vHC: $Z=-0.77$, $p=0.44$, Wilcoxon signed-rank test).

incorrect – with correct and incorrect referring to the oder-cued response. The odor-cued response of the animals was independent of their alternation behavior (69% trials correct; 63% trials alternating; $\chi^2(1,1207) = 0.01$, $p=.92$). When analyzing LFP recorded on the stem arm in the different types of trials, coherence between pairs of regions in the mPFC-dHC-vHC network in the stem arm was not different between correct and incorrect odor-

guided trials in this task (mPFC-dHC: Z=-0.48, p=0.63; mPFC-vHC: Z=-0.05, p=0.96; dHC-vHC: Z=-0.77, p=0.44, Wilcoxon signed-rank test) (**Fig 2.7B**). However, we found that coherence was significantly higher during alternating compared to non-alternating trials (mPFC-dHC: Z=2.80, p<.01; mPFC-vHC: Z=2.37, p<.05; dHC-vHC: Z=2.40, p<.05, Wilcoxon signed-rank test) (**Fig 2.7A**). These results are consistent with reports that prefrontal-hippocampal theta synchrony increases at the choice-point of a Y- or W-maze during a spatial alternation task (Benchenane et al., 2010; Jones & Wilson, 2005).

Discussion

Although it is well established that respiration-entrained oscillations are propagated from the OB to other cortical areas, it is unclear to what extent these respiration-entrained oscillations get coupled to endogenous theta oscillations in the prefrontal-hippocampal regions. To investigate the coordination of respiration-entrained oscillations in the OB and of theta oscillations in the prefrontal-hippocampal circuit, we analyzed LFP signals from the OB, mPFC, dHpC and vHpC during an odor-cued working memory task. We found that respiration-entrained oscillations in the OB were distributed across the 3-12 Hz frequency range within each task phase, including phases when animals moved and phases when animals were predominantly immobile. By examining these task phases separately, we were able to test whether movement-related and sensory-evoked theta oscillations in the prefrontal-hippocampal couple with respiration-entrained oscillations. For movement-related theta, we found that OB and cortical oscillations either occurred at different frequencies or, when occurring at similar frequencies remained uncoupled from

respiration-entrained oscillations in the OB. Similarly, this was also observed for sensory evoked theta oscillations during odor sampling periods. Taken together, our results indicate that respiration-entrained oscillations that are propagated from the OB to prefrontal-hippocampal regions do not become coupled to local theta oscillations even during odor sampling periods when olfactory inputs can be assumed to strongly drive information processing. RROs in the prefrontal-hippocampal regions therefore remained independent from canonical theta oscillations and increased coupling of the oscillations does not appear to serve as a conduit for information processing in an odor-cued working memory task. Rather, we confirmed the previous finding that movement-related theta oscillations within the prefrontal-hippocampal network become more coherent when the spatial component of this task guides the behavioral responses.

It has long been known that rodent breathing frequencies can vary in a wide range but their relation to behavior has not been firmly established. Mice have a "passive" breathing frequency of 1-4 Hz during quiescence (Jessberger et al., 2016; Wesson et al., 2011). Upon exposure to a novel odor, mice begin "active" sniffing at a high frequency of 4-12 Hz (Jessberger et al., 2016; Wesson et al., 2008; Wesson et al., 2011). Such a modulation of respiration frequencies during odor sampling has been thought to be the basis for odor processing in lower-order olfactory circuits (Wesson et al., 2008). Indeed, sniffing frequency changes the number of odor molecules arriving at the OSNs, thereby modulating the response of OSNs at higher sniffing frequencies (Courtiol et al., 2011). However, further investigations of the role of sniffing frequencies in odor information processing has revealed that mice have varied strategies in terms of sniffing frequencies

(Reisert et al., 2020; Wesson et al., 2008). While sniffing frequencies do increase in response to a novel odor sampling, mice are able to perform "easy" as well as "difficult" odor discrimination tasks without a significant increase in their sniffing frequencies compared to baseline (Wesson et al., 2008; Wesson et al., 2009). Moreover, the relationship between sniffing frequencies and odor guided behavior is confounded by multiple factors such as locomotion and reward expectation, both of which lead to increased sniffing rates (Bramble & Carrier, 1983; Clarke, 1971; Hérent et al., 2020; Wesson et al., 2008). Our results are consistent with a variable relation between breathing frequencies and behavior because we find that a similarly broad range of RROs can occur in any of the behavioral phases in an odor-guided working memory task.

Although oscillations in the 4-12 Hz band are broadly referred to as theta, it is well established that theta oscillations in the hippocampus are of at least two types – type I and type II. Type I theta is atropine-insensitive and is movement-related (Kramis et al., 1975; Vanderwolf, 1969). Power and frequency of type I theta oscillations have been shown to increase with higher running speeds (Feder & Ranck, 1973; Kuo et al., 2011). Our analysis of movement-related theta oscillations in the return and stem arms revealed that theta oscillations during those periods showed similar relations to movement as type I theta (Fig S3). On the other hand, type II theta is atropine sensitive, and is unrelated to movement (Kramis et al., 1975; Vanderwolf, 1969). Type II theta is elicited when the animal is exposed to arousing, vigilant and aversive conditions, such as a predator's smell (Sainsbury et al., 1987). Our recording of sensory-evoked theta oscillations during the odor sampling period is akin to type II theta oscillations although we did not test the atropine sensitivity

of these oscillations. However, we confirmed that these theta oscillations occur while the mice's nose is held in the odor port and immobile, which suggests that theta oscillations during this task phase fulfill at least one of the criteria for type II theta.

Our analysis suggests that movement-related theta oscillations in the prefrontal-hippocampal network do not become coherent with the respiration-entrained rhythm in the OB. In their original paper, Vanderwolf & Szechtman, (1987) recorded nasal thermistor signals as well as LFP from the OB and dorsal hippocampus and reported that the hippocampal movement-related theta (termed RSA at the time) do not couple to the respiration rhythm during exploration. Along the same line, Nguyen Chi et al., (2016) reported that the RROs are a separate oscillation from the canonical movement-related oscillation during running by studying the depth profiles of these oscillations. They suggested that RROs and movement-related theta oscillations can co-exist during running but did not comment on their coupling. In contrast, Tort et al., (2018) found that movement-related theta oscillations within the hippocampus and the medial prefrontal cortex were coherent with the respiration rhythm during exploration. While it is therefore possible that a theta oscillation at a subset of recording sites (e.g., in DG) in the hippocampus are coupled with olfactory oscillations, the high-amplitude theta signal that we recorded does not seem to show this property.

Furthermore, our data are also consistent with earlier studies that suggest that sensory-evoked hippocampal theta oscillations are not coupled to respiration-coupled OB oscillations. While (Macrides et al., 1982) reported that during odor sampling, theta oscillations in the hippocampus couple with respiration rhythm during the initial stages of

learning an odor discrimination reversal task, they found that coherence between these oscillations was low in expert animals. Our study includes analysis of well-trained animals only, which could explain the decreased coherence. On the other hand, (Kay, 2005) showed that hippocampal theta oscillations and the sniffing rhythm were coherent during odor sniffing and that this coherence was positively correlated to performance in a two-odor discrimination task, but not in extended runs of single odor conditional-stimulus-positive trials. This provides additional evidence that coupling between sensory-evoked theta oscillations and the respiration-entrained oscillation is dependent on task difficulty or novelty. Taken together, these results indicate that the coupling of sensory-evoked theta oscillations with the respiration rhythm could potentially aid in sensorimotor integration during difficult odor-discrimination tasks or during early phases of learning even in easy discrimination tasks.

Our results concur with existing narratives that respiration-entrained oscillations are detected in the prefrontal-hippocampal areas when the respiration frequencies do not match the frequency of theta oscillations in the hippocampus. This detection has been reported to be more obvious when respiration frequencies are lower than theta oscillations in the hippocampus (Nguyen Chi et al., 2016), but RROs can also be detected even when respiration frequencies are higher than theta frequencies. However, a majority of investigations have studied periods of low respiration frequency (< 6 Hz) (Lockmann et al., 2016; Nguyen Chi et al., 2016; Yanovsky et al., 2014). Could it be that respiration-entrained oscillations in the OB are transmitted differently to downstream cortical areas based on frequency? Or that our detection capabilities preclude us from observing

oscillations higher in frequency? Our comparison of trials with overlapping and non-overlapping RRO and theta frequencies (Fig 3) indicates that respiration-entrained OB oscillations did not get coupled to prefrontal-hippocampal oscillations during trials with overlapping RRO and theta frequency (Fig 4, 5). Our interpretation of these results is that RROs do not couple to canonical theta. However, since our overlap trials are primarily those in which the predominant frequency of OB oscillations is above 6 Hz (Fig 3), our results could be interpreted as RROs >6Hz do not couple to theta oscillations. Some evidence for this comes from the finding that while mitral and tufted cells in the OB are entrained to the respiration rhythm at low frequencies (up to 6Hz), they fire tonically at higher respiratory frequencies (6-12 Hz) (Kay & Laurent, 1999).

Previous studies have suggested that the respiration-entrained oscillation is a global signal that synchronizes activity across multiple brain regions and contributes to sensorimotor integration in a context dependent manner. However, these studies have performed these analyses in anesthetized mice, mobility or immobility or when they performed head fixed tasks (respiration frequencies less than 6 Hz). Our results indicate no functional significance for such a global respiration-entrained oscillation, and it remains an open question whether broad coupling of these oscillations across brain regions is used for some types of memory-related computations.

Materials and Methods

Subjects

Eight mice (VGAT-cre 129S6(FVB)-Slc32a1$^{tm2(cre)Lowl}$/MwarJ, Jackson Labs; n = 4 male, n = 4 female) of age 4 months, weighing between 20-30 grams were used as subjects. All mice were housed in a reverse 12 hr dark/light cycle (lights off at 8 am). Mice were restricted to 85-90% of their *ad libitum* weight and given full access to water. All the training and testing were conducted during the dark phase. All procedures were conducted in accordance with the University of California, San Diego Institutional Animal Care and Use Committee.

Surgery

Mice were anesthetized with isoflurane (induction: 3%, maintenance: 1.5-2%) and mounted in a stereotaxic frame (David Kopf Instruments, Model 1900). The scalp was cleaned and retracted using a midline incision and the skull was leveled between bregma and lambda. Five holes were drilled in the skull to attach anchor screws. A hole was drilled above the cerebellum to place the ground screw. Craniotomies were performed over four brain regions on the right hemisphere (OB: +4.2mm A/P, 0.6mm M/L; mPFC: +1.8-2mm A/P, 0.4mm M/L; dHpC: -1.9mm A/P, 2.0mm M/L; vHpC: -3.3mm A/P, 3.5mm M/L) and dura was removed. Wires were implanted in the four brain regions (OB: -1.2mm D/V; mPFC: -1.4mm D/V; dHpC: -1.8mm D/V; vHpC: -3.5mm D/V) to record local field potentials. The wires were threaded through an EIB-18 board. The implant was secured with dental cement. Postoperative care was administered as needed and mice were allowed

to recover for a minimum of 5 days.

Histological Procedures

Mice were perfused with 0.1 M phosphate-buffered saline (PBS) followed by 4% paraformaldehyde in PBS solution. Brains were post-fixed for 24 hours in 4% paraformaldehyde and then cryoprotected in 30% sucrose solution for 2 days. Brains were then frozen and sliced into 40 μm coronal on a sliding microtome. Sections were mounted on electrostatic slides, stained with cresyl violet and coverslipped with Permount (Fisher Scientific, SP15500) to visualize recording locations. Slides were imaged using a virtual slide microscope (Olympus, VS120).

Olfactometer and Odor delivery

A custom plastic odor port was machined with the help of the machine shop on the University of California, San Diego campus. Two IR LEDs (transmitter and receiver) were placed at the entrance of the odor port to detect nose pokes. These LEDs were connected to an Arduino board (Arduino Mega 2560) which was programmed to detect nose pokes and deliver an odor through the custom-made olfactometer. One of the two odors was pseudo-randomly delivered on each trial, with an inter trial interval of 2 seconds, to prevent setting off the odor delivery twice within a single trial. A custom written MATLAB script was used to deliver the odor as well as to send a TTL pulse to the Neuralynx acquisition system to timestamp the odor delivery, nose poke in and nose poke out. A hole was drilled at the bottom of the odor port to deliver the odor at a flow rate of up to 1L/min. Two neutral

odors (ethyl acetate and isoamyl acetate) were used in the task. These odors were freshly prepared daily in mineral oil (1:5 ratio by volume).

Behavior

Mice were trained on an odor-cued working memory task. The room was dimly lit and had stable environmental cues. The task was performed on a figure-8 maze that was 50 cm above the ground and had dimensions of 75 cm by 50 cm. The runway on the figure-8 maze had a width of 5 cm. A custom-made olfactometer was placed on one end of the stem arm. The maze was cleaned with 70% alcohol after each animal used the maze. Animals were trained in phases. On the first day, animals were allowed to freely explore the maze for 10 minutes to habituate them. After habituation for one day, animals started the first phase of training. In the first phase (training), animals were gently guided to the odor port to break an IR beam at the entrance of the odor port upon which an odor was delivered. Animals were required to sniff the odor and run to the other end of the stem arm and were forced to make the correct choice. They were then rewarded with a single chocolate sprinkle (Betty Crocker Parlor Perfect Chocolate Sprinkles) at the reward zone. Care was taken to place the chocolate sprinkle at the reward location only after the animal made its choice. Animals performed 60 trials per day. Once animals learned to nose poke in the odor port and run to the opposite end of the stem arm without guidance in all 60 trials on two consecutive days, they were ready for the second phase. In the second phase (testing), animals performed the task without guidance to nose poke into the odor port and turned at the other end of the stem arm without compulsion. Responses on all 60 trials were

recorded and analyzed.

Electrophysiological recordings

Local Field Potentials (LFP) were recorded using chronically implanted wires. Implanted wires were threaded through a head-mounted preamplifier and connected via a tether to a 32-channel digital data acquisition system (Neuralynx, Bozeman, MT). Continuous LFP was sampled at 32000 Hz and band-pass filtered between 0.1 and 1000 Hz. Position data of a red and a green LED located on either side of the head-mounted preamplifier were tracked by a video camera at a sampling frequency of 30 Hz to determine the spatial location of the animals while they performed the task.

LFP Analysis

Raw LFP signals were down-sampled to 2000 Hz and a Morlet wavelet of width ratio = 6 was used to determine the power and phase of the oscillations at 30 log-spaced frequencies in the 3-20 Hz range. An average spectrogram was constructed for each maze zone in each trial. For each frequency, phase differences between pairs of oscillations were calculated, and coherence in each maze zone was computed as the length of the resultant vector of phase differences in that zone. For analysis involving predominant frequencies within a region, a peak was detected in the 3-12 Hz for RROs and in the 6-12 Hz range for movement-related and sensory-evoked theta oscillations. If no peak was detected, that trial was omitted from analysis for that maze zone.

Statistics

All statistics were performed using built-in functions in MATLAB (R2019b). Non-parametric tests such as Kruskal-Wallis, Friedman and Wilcoxon tests were performed. Corrections for multiple tests were performed using Holm-Bonferroni method.

Code availability

Code can be accessed at https://github.com/SunandhaSrikanth.

Acknowledgements

We thank members of the Jill Leutgeb and Stefan Leutgeb labs for valuable comments and suggestions at various stages of this project. We thank Dr. Cory Root for help with the custom olfactometer set up. We also thank Mr. Vignesh Srinivasan for help with setting up the odor port. This research was supported by grants from the National Institute of Health (NS102915, NS097772 and MH119179).

Competing interests

The authors declare no competing interests.

Acknowledgements

We thank members of the Jill Leutgeb and Stefan Leutgeb labs for valuable comments and suggestions at various stages of this project. We thank Dr Cory Root for help with the custom olfactometer set up. We also thank Mr. Vignesh Srinivasan for help

with setting up the odor port. This research was supported by grants from the National Institute of Health (NS102915, NS097772 and MH119179).

Chapter 2, in full, is material that is currently being prepared for submission for publication by Srikanth, Sunandha; Le, Dylan; Hu, Yudi; Leutgeb, Jill K.; and Leutgeb, Stefan. The dissertation author was the primary researcher of this material.

Appendix 2.1: Supplemental Figures

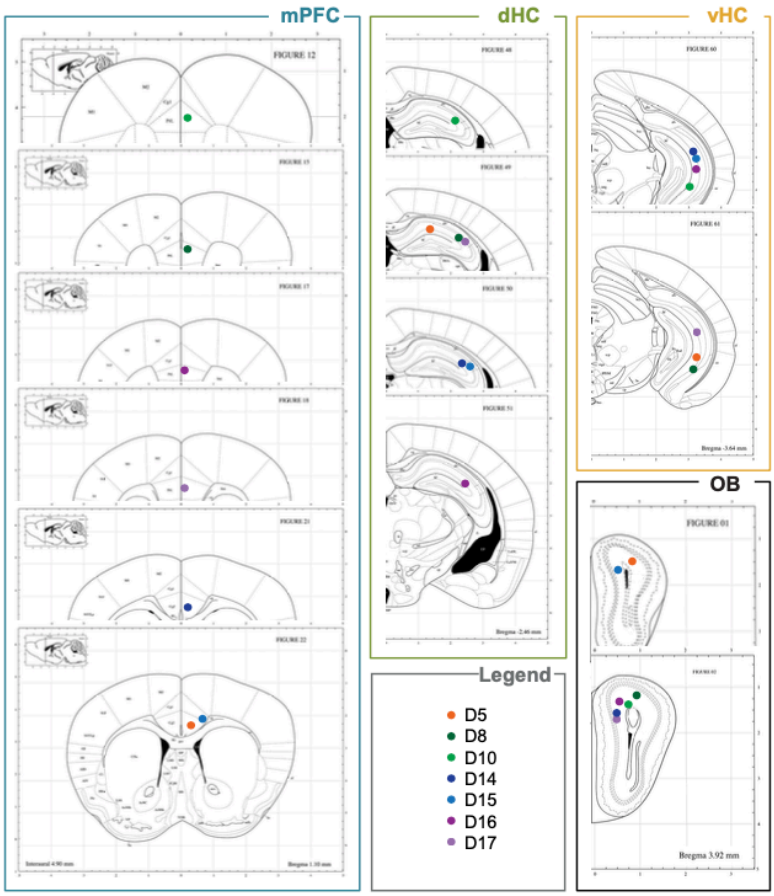

Supplemental Figure 2S.1 – Electrode recording locations.

Recording electrode locations in n=7 mice are shown. Colored dots indicate the recording locations in the different animals used in the study. Electrodes were histologically confirmed to be placed in the OB, prelimbic, infralimbic and anterior cingulate areas of the mPFC and CA1 areas of the dHC and the vHC.

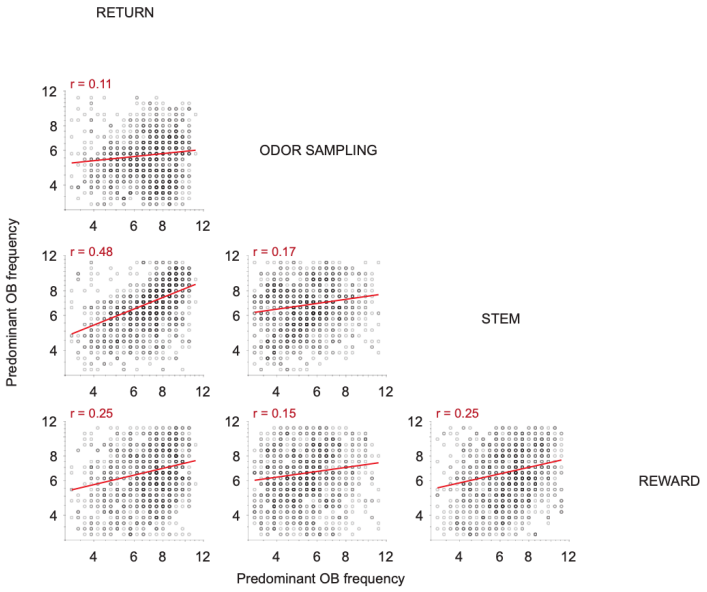

Supplemental Figure 2S.2 - Weak correlations between predominant OB frequencies in different task phases.

Scatter plots of predominant OB frequencies during different task phases in each trial. Correlations between predominant OB frequencies during different task phases were weak.

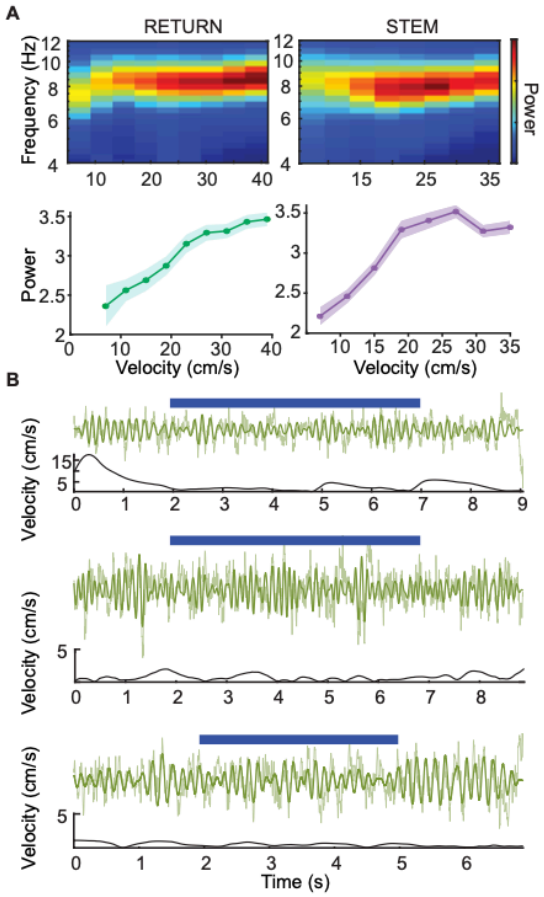

Supplemental Figure 2S.3 – Movement-related and sensory-evoked theta oscillations in the dHC.

A. (Up) Mean spectrograms during periods of running on the return arms and stem arm, displaying the distribution of power and frequency of movement-related theta oscillations across running speeds are shown. (Down) Corresponding average power (±SEM) across running speeds is displayed. **B**. Example raw (light green) and filtered (dark green) LFP traces of sensory evoked theta oscillations in the dHC are shown in three different trials. Blue bars represent the time of odor sampling. Velocity traces accompanying each raw LFP trace show the velocity of the animal during the same time period.

III.

COORDINATION OF SPIKE TIMING BY THETA OSCILLATIONS WITHIN THE MEDIAL PREFRONTAL CORTEX AND THE HIPPOCAMPUS

Abstract

Brain oscillations provide a synchronizing signal for the coordination of spike timing across brain regions, thus supporting cognitive functions such as working memory. Theta oscillations (7-9 Hz) in the hippocampus that are generated by the medial septal area (MSA) have been found to be important during learning and memory. In addition, interactions between the hippocampus and the prefrontal cortex have been established to play a role in spatial working memory. In this study, we probe the mechanisms of these interactions by manipulating the precise timing of theta oscillations through optical stimulation of the MSA. We show that local field potentials in the hippocampus as well as the medial prefrontal cortex are strongly entrained to optical stimulation of the MSA at accelerated (12 Hz), decelerated (4 Hz) and endogenous (8Hz) theta frequencies. However, only a small subset of local neuronal populations within the medial prefrontal cortex are entrained to the artificially stimulated oscillations. Moreover, this entrainment is stronger upon stimulation at 8 Hz compared to 4 Hz or 12 Hz. We also found that entrainment to the artificially paced oscillations was stronger during the encoding and maintenance phases of spatial working memory and nearly non-existent during the retrieval phase. Spatial firing

properties of medial prefrontal cortex neurons remained unaltered in response to stimulation at any of the three frequencies. These results suggest that neuronal computations between the medial prefrontal cortex and the hippocampus are predominantly coordinated by oscillations during task phases when information is encoded and maintained.

Introduction

Oscillations in the brain provide a clocking mechanism that aids in synchronizing neuronal activity (Buzsáki & Draguhn, 2004). Slow brain oscillations can integrate information across large spatial scales by coordinating the timing of networks of neurons. Such synchronized activity in disparate brain regions provide a conduit for long-range communication and information transfer between these regions, thus facilitating cognitive processing. While there exists a vast literature that establishes correlations between precisely timed oscillatory activity and cognition, investigations into causative relationships between the two are sparse.

The hippocampal theta rhythm (4-12 Hz) has been attributed to various complex behaviors and cognitive processes including spatial navigation and working memory (Winson, 1978). These hippocampal theta oscillations have been firmly established to be paced by GABAergic pacemaker neurons within the medial septal area (MSA), which project onto interneurons within the hippocampus (Bland, 1986; Bland & Bland, 1986; Gaztelu & Buño, 1982; Mitchell et al., 1982; Yoder & Pang, 2005). Lesioning the MSA causes an abolishment of theta oscillations within the hippocampus (HpC) as well as

behavioral impairments in tasks that are dependent on spatial working memory such as the radial maze task and the Morris water maze task (Mitchell et al., 1982; Mizumori et al., 1989; Mizumori et al., 1990; Winson, 1978; Yoder & Pang, 2005). Theta oscillations have been proposed to facilitate memory processes by synchronizing the activity of neuronal populations (Royer et al., 2010; Shirvalkar et al., 2010; Skaggs et al., 1996; Wang et al., 2015; Zutshi et al., 2018). However, pharmacological manipulations and lesion studies cause changes to the excitability of the neurons and do not allow for a selective assessment of the role of the timing of the oscillations. More recently, our lab has established that acceleration of septally paced theta oscillations to beyond the endogenous range (10 Hz and above) can cause a behavioral impairment in a hippocampal-dependent version of the spatial alternation task. This effect was particularly pronounced when stimulation was turned on during task phases when information was being encoded.

Besides local neuronal populations with the HpC, neuronal populations in the medial prefrontal cortex (mPFC) are also modulated by the hippocampal theta rhythm (Hyman et al., 2005; Jones & Wilson, 2005; Siapas et al., 2005; Zielinski et al., 2019). The prefrontal-hippocampal oscillatory interactions in the theta range have been correlated to performance in spatial working memory tasks in rodents (Benchenane et al., 2010; Jones & Wilson, 2005; Zielinski et al., 2019). Specifically, prefrontal-hippocampal oscillatory interactions have been found to be theta modulated during the retrieval or decision-making phase of spatial memory. However, hippocampal inputs to the mPFC that provide a spatial signal modulate prefrontal activity during the encoding phase of a spatial working memory task (Spellman et al., 2015).

It is thus crucial to understand the role of precisely timed theta oscillations in mediating prefrontal-hippocampal interactions during different phases of spatial working memory. Therefore, we optogenetically manipulated PV+ interneurons in the MSA of to either accelerate (to 12 Hz), decelerate (to 4Hz) or lock the frequency of theta oscillations within the endogenous frequency range (8 Hz), while mice performed a delayed spatial alternation task on a figure-8 maze. We simultaneously recorded LFP signals from the hippocampus as well as single unit activity and LFP signals from the mPFC. We confirmed that both hippocampal and medial prefrontal theta oscillations were paced at all three stimulation frequencies. Then, we examined the spatial and temporal firing patterns of mPFC single units in response to paced oscillations. Further, we studied stimulation-induced changes in single-unit firing patterns specifically during the encoding and retrieval phases of the task.

Results

To test the role of precisely timed theta oscillations in mediating hippocampal-prefrontal interactions, we adopted an optogenetic approach as previously described (Zutshi et al., 2018). Briefly, we virally expressed cre-dependent channelrhodopsin (cre-ChR2) in PV+ pacemaker cells in the medial septal area (MSA) of PV-cre mice (**Fig 3.1B**; ChR2 group n=6 mice; 3M, 3F, age: 3-4mo). With ChR2 expression in MSA-PV cells,

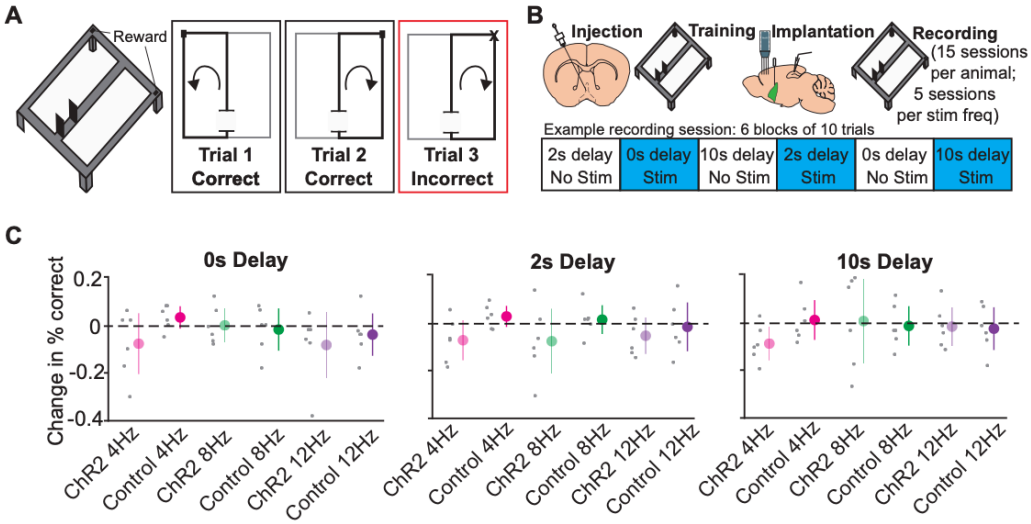

Figure 3.1 – Task set up, experimental timeline and behavior results.

A. Animals (n=6 ChR2 group, n=7 Control group) were trained on a delayed version of a spatial alternation task. Animals were trained to make alternating choices between left and right arms on a figure-8 maze. To make the task dependent on the hippocampus, a delay was introduced (2 s or 10 s). **B**. Timeline of the experiment. **C**. Change in performance (% correct in stim - % correct in no stim) for each delay condition and each stimulation frequency for ChR2 animals and control animals. Trends of impairment were observed in response to 12 Hz stimulation.

blue light of a specific frequency targeted at the MSA activates PV+ neurons, thereby pacing theta oscillations within the hippocampus (HpC) via a disinhibition mechanism. To control for effects of light and viral expression, we used a second group of PV-cre mice and virally expressed a cre-dependent fluorophore (cre-GFP) in PV+ interneurons within the MSA (Control group n=7 mice; 3M, 4F, age: 2-4mo). Mice were trained on a spatial alternation task (**Fig 3.1A**). In addition to the continuous version of the alternation task, we introduced delays (2 s or 10 s) to make the task hippocampus dependent. Animals were thus tested on three delay conditions (0 s, 2 s, 10 s). Each session was comprised of 60 trials, divided into 6 blocks of 10 trials. The six blocks consisted of two repetitions of the

three delay conditions with the order of the delays randomized on each day. Stimulation was turned on during every second block such that each delay condition occurred twice, once with and once without stimulation (**Fig 3.1B**). We performed stimulation with three frequencies (4 Hz, 8 Hz and 12 Hz), using only one stimulation frequency per day. Each animal had 15 recording sessions with 5 days per stimulation frequency, and the order of the frequencies was randomized for each animal.

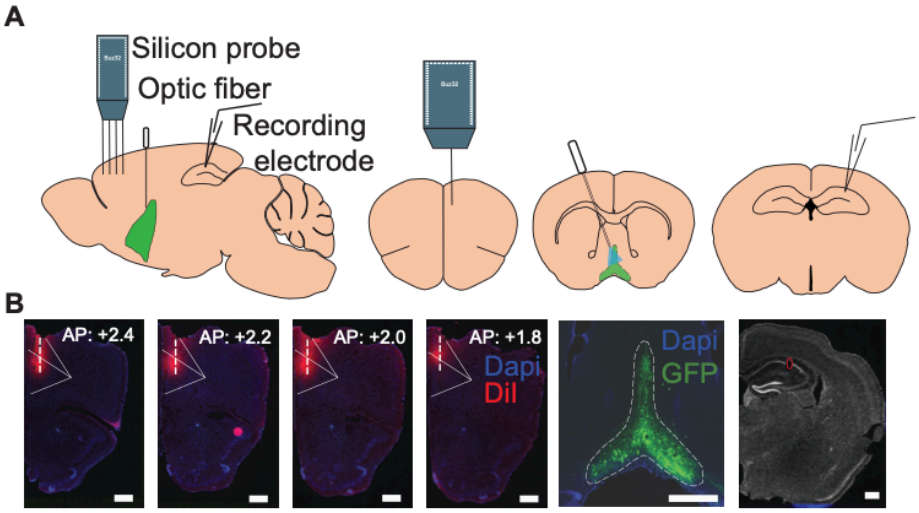

Figure 3.2 – Recording Schematic and histology.

A. While animals performed the spatial alternation task, a 32-channel silicon probe was used to record LFP and single unit activity within the mPFC and an electrode was used to record LFP signals from the HpC. An optic fiber was implanted such that it targeted the MSA. **B**. Histology examples are shown. The silicon probe was coated with DiI dye before implantation and fluorescence was imaged post mortem to track the probe locations. We confirmed that MSA showed good expression of cre-ChR2-GFP in all animals. Electrode locations were histologically confirmed to be located in the CA1 layer of the HpC. Scale bar: 500 μm.

Our lab has previously demonstrated that accelerating theta oscillations to beyond endogenous frequency ranges (10 Hz and above) resulted in behavioral impairments in the

delayed (hippocampus-dependent) version of the spatial alternation task, while decelerating theta oscillations did not cause impairments (Quirk et al., 2021, in press). We first attempted to replicate these results in our study. While we observed similar trends towards impairment upon accelerating theta oscillations to 12 Hz in the ChR2 group, the results were not statistically significant (**Fig 3.1C, Table 3.1, Table 3.2**). We attributed these differences from the Quirk et al., study to over-training and low animal numbers (n = 6 ChR2 animals in our study versus n = 40 ChR2 animals in the Quirk et al., 2021 study).

Table 3.1. Statistical analysis of ChR2 animals' performance across all frequencies and delays.

Paired t-tests were performed on the performance of ChR2 animals (n=6). Holm-Bonferroni correction was used to correct the p values obtained from the paired t-tests. Corrected p values showed no significance.

	Holm-Bonferroni correction, p values		
	4 Hz n = 6	**8 Hz n = 6**	**12 Hz n = 6**
No delay	0.22	0.94	0.23
2s delay	0.13	0.29	0.21
10s delay	0.26	0.99	0.54

Table 1.2. Statistical analysis of control animals' performance across all frequencies and delays.

Paired t-tests were performed on the performance of control animals (n=7). P values showed no significance.

	Paired t-test, p values		
	4 Hz n = 7	**8 Hz n = 7**	**12 Hz n = 7**
No delay	0.34	0.48	0.49
2s delay	0.12	0.78	0.57
10s delay	0.93	0.71	0.72

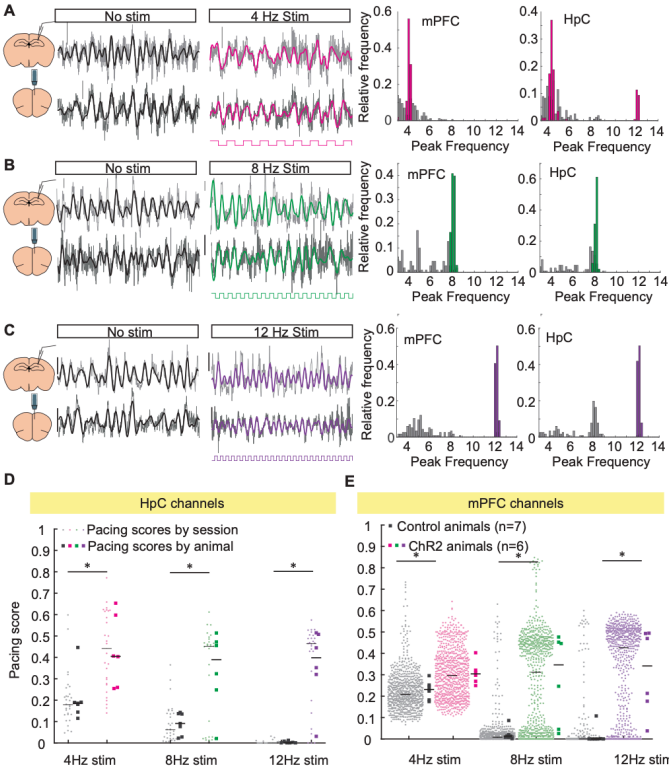

Figure 3.3 – LFPs in the HpC and the mPFC were paced in response to septal stimulation at 4 Hz, 8 Hz and 12 Hz.

Two-second-long raw (grey lines) and filtered LFP (thick black, thick colored lines) signals recorded from the HpC and mPFC during a 4 Hz (**A**), 8 Hz (**B**) and 12 Hz (**C**) stimulation sessions (left: no stim, right: stim) are shown. Square wave represents the stimulation pulses. Histograms of peak frequencies calculated in 2-s windows of time-frequency spectrograms are plotted for no stim and stim conditions (**A-C**). **D**. Pacing scores of hippocampal channels are shown (dots: session-wise score, squares: animal-wise score). **E**. Pacing scores of prefrontal channels (dots: session-wise and channel-wise score, squares: animal-wise score). Black dots and squares are data from control animals while colored dots and squares are from ChR2 animals. Note that there are more data points for the mPFC channels because each session recorded data from 31 mPFC channels and one HpC channel.

Pacing of MSA PV+ interneurons reliably paced theta oscillations in the HpC at 4 Hz, 8 Hz and 12 Hz

While the animals performed the delayed spatial alternation task, we simultaneously recorded single units and local field potentials from the mPFC (prelimbic, PL and infralimbic, IL areas) as well as local field potentials from the HpC (**Fig 3.2A, B, C**). We first confirmed that animals in the ChR2 group exhibited efficiently paced theta oscillations in the hippocampus in response to three stimulation frequencies (4 Hz, 8 Hz and 12 Hz). A visual examination of raw LFP traces in the HpC revealed oscillations locked to the stimulation frequency (**Fig 3.3A, B, C**). In order to quantify the efficiency of pacing, we employed the use of pacing scores (see Methods). In each session, the peak frequency of the HpC theta oscillations in 2-second-long moving windows were calculated, and a histogram of these peak frequencies was plotted (**Fig 3.3A, B, C**). When stimulation was turned off, a cluster around 8 Hz (endogenous theta frequency) was observed. However, when stimulation was turned on, a cluster around the stimulation frequency was observed (**Fig 3.3A, B, C**). The peak of the histogram in a 2 Hz range around stimulation frequency was taken to be the HpC pacing score for that session. Pacing scores calculated for mice in the ChR2 group were higher than those for mice in the control group (**Fig 3.3D**) (4 Hz: $p < .01$, $Z = -14.8$, Wilcoxon Rank Sum Test; 8 Hz: $p < .01$, $Z = -12.5$, Wilcoxon Rank Sum Test; 12 Hz: $p < .01$, $Z = -26.6$, Wilcoxon Rank Sum Test). Note that 4 Hz and 8 Hz pacing scores in the control group are higher than that of 12 Hz due to endogenous low frequency oscillations in the HpC.

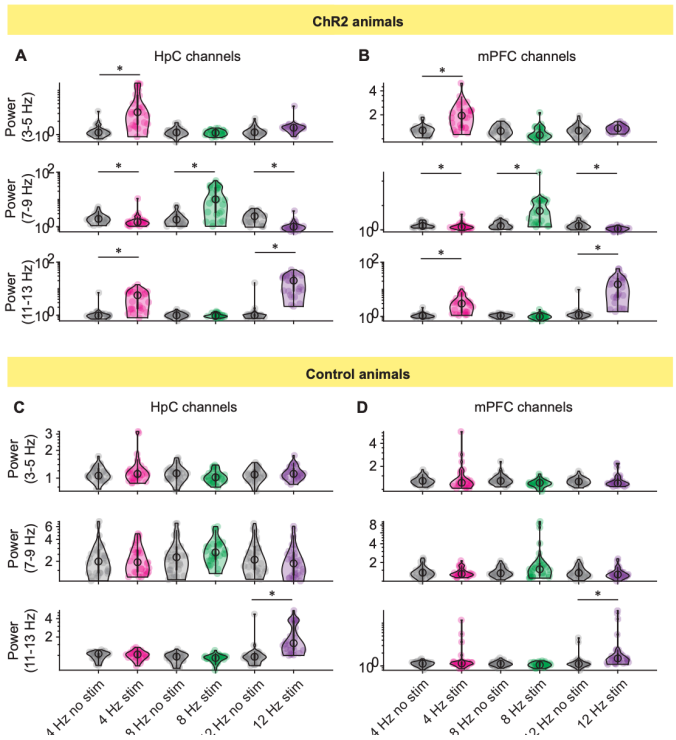

Figure 3.4 – Septal stimulation exclusively reduced the power of endogenous theta oscillations whereas the power of endogenous ~4-5 Hz oscillations within the mPFC remained unaffected.

A. Peak power in a ±1 Hz range around the stimulation frequency (top: 3-5 Hz, middle: 7-9 Hz and bottom: 11-13 Hz) for each HpC channel was calculated and plotted. Increased power was observed at the stimulation frequency in response to stimulation (4Hz: $p < .01$, $Z = -4$, Wilcoxon Signed Rank Test; 8 Hz: $p < 0.01$, $Z = -4.6$, Wilcoxon Signed Rank Test, 12 Hz: $p < 0.01$, $Z = -4.6$, Wilcoxon Signed Rank Test), whereas power of endogenous theta oscillations was decreased in response to 4 and 12 Hz stimulation. **B**. Peak power in a ±1 Hz range around the stimulation frequency (top: 3-5 Hz, middle: 7-9 Hz and bottom: 11-13 Hz) for each mPFC channel was calculated, averaged per session and plotted. Increased power was observed at the stimulation frequency in response to stimulation (4 Hz: $p < .01$, $Z = -4.2$, Wilcoxon Signed Rank Test; 8 Hz: $p < .01$ $Z = -4.5$, Wilcoxon Signed Rank Test; 12 Hz: $p < .01$, $Z = -4.6$, Wilcoxon Signed Rank Test), whereas power of endogenous theta oscillations was decreased in response to 4 Hz and 12 Hz stimulation (4 Hz: $p = 0.046$, $Z = 2.52$, Wilcoxon Signed Rank Test; 12 Hz: $p < .01$, $Z = 4.1$, Wilcoxon Signed Rank Test). Power of endogenous ~4-5 Hz oscillations remained unaltered in response to 8 Hz and 12 Hz stimulation (8 Hz: $p = 0.18$, $Z = 1.89$, Wilcoxon Signed Rank Test; 12 Hz: $p = 0.22$, $Z = -1.22$, Wilcoxon Signed Rank Test). Four Hz optical stimulation also increased power in the 11-13 Hz band but it is likely due to the emergence of harmonics ($p < .01$, $Z = -4.18$, Wilcoxon Signed Rank Test) **C and D**. Same as **A** and **B** but for control animals.

Pacing at 4 Hz overrides endogenous 4 Hz oscillations within the mPFC

After confirming that HpC theta oscillations are paced by all three stimulation frequencies, we asked whether mPFC theta oscillations are similarly paced. Pacing scores were calculated for each mPFC channel during a recording session using the same procedure as for HpC LFP. Pacing scores were higher in the ChR2 group compared to the control group for all frequencies (**Fig 3.3E**) (4 Hz: $p < .01$, $Z = -4.7$, Wilcoxon Rank Sum Test; 8 Hz: $p < .01$, $Z = -3.5$, Wilcoxon Rank Sum Test; 12 Hz: $p < .01$, $Z = -6.3$, Wilcoxon Rank Sum Test). Note that in addition to theta oscillations, there are prominent endogenous ~4-5 Hz oscillations in the mPFC. Therefore, pacing scores of 4 Hz stimulation sessions were only modestly increased in ChR2 animals compared to the control animals (**Fig 3.3E**). These results suggest that our optogenetic approach to pacing theta oscillations is effective in not just the hippocampus, but also in the mPFC.

Pacing at 8 Hz and 12 Hz caused shifts in theta frequency to the stimulation frequency while endogenous 4 Hz oscillations in the mPFC remained intact

Since the mPFC LFP has predominant oscillations in the ~4-5 Hz range as well as theta oscillations, we asked whether our manipulation of septally paced oscillations had effects on the ~4-5 Hz oscillations. To test this, we compared the power of the endogenous ~4-5 Hz oscillations during stimulation-on and stimulation-off periods when stimulating at either 8 Hz or 12 Hz. We did not include the 4 Hz stimulation frequency because this would yield the trivial result that stimulation has effects within an overlapping frequency band. Our analysis revealed that the power of the endogenous ~4-5 Hz oscillation in the mPFC remained intact when 8 and 12 Hz stimulation was turned on (**Fig 3.4A**) (8 Hz: $p = 0.18$,

Z = 1.89 , Wilcoxon Signed Rank Test; 12 Hz: p = 0.22, Z = -1.22, Wilcoxon Signed Rank Test). This indicates a separate mechanism for generation of the ~4-5 Hz oscillation as has been proposed previously (Fujisawa & Buzsáki, 2011). It also implies that effects of our manipulation of septally paced oscillations are confined to only theta oscillations.

Paced oscillations in the mPFC were coherent with paced oscillations in the HpC

To further confirm whether the pacing of theta oscillations in the HpC and the mPFC generates coupled oscillations, we calculated the coherence of the paced oscillations between the two brain regions. Coherence at the stimulation frequency was higher during stimulation on compared to stimulation off periods, for 8 Hz and 12 Hz stimulation (**Fig 3.5**). Although the 4 Hz stimulation also increased coherence between the two regions, this effect was modest (4 Hz: p = 0.059, Z = -2.4, Wilcoxon Signed Rank Test). This smaller effect with 4 Hz stimulation could be explained by competing endogenous oscillations in the ~4-5 Hz range.

Pacing at accelerated or decelerated frequencies had no significant effects on spatial firing properties of mPFC neurons

We classified single units recorded from the mPFC into wide-spiking (n = 594 putative principal cells) and narrow-spiking neurons (n = 77 putative interneurons) based on two waveforms characteristics (peak-to-trough duration and spike width) (**Fig 3S.2B**). We employed a Gaussian Mixture Model (GMM) to perform the classification. Cells with

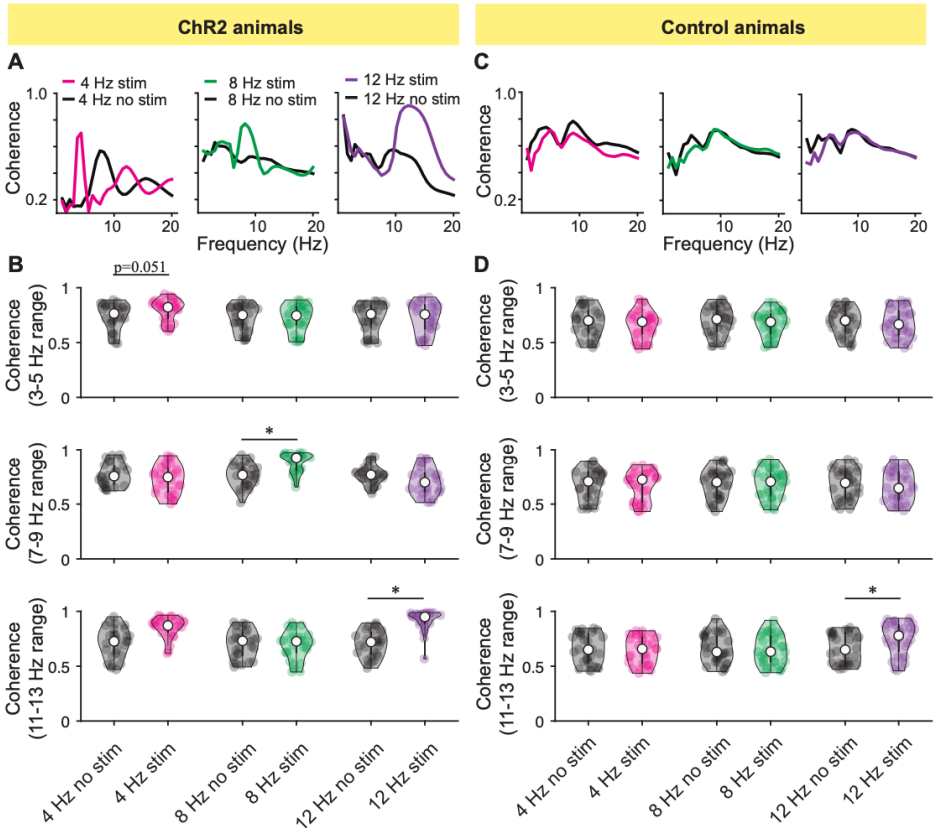

Figure 3.5 – Septally paced oscillations within the HpC and the mPFC were coherent with one another.

A. Example coherence spectra between HpC and mPFC channels for 4 Hz (left), 8 Hz (middle) and 12 Hz (right) stimulation sessions are shown for ChR2 animals (no stim: black; 4 Hz stim: pink; 8 Hz stim: green; 12 Hz stim: purple). Peak coherence was observed at the stimulation frequency. **B**. Peak coherence in a ±1 Hz range around the stimulation frequency (top: 3-5 Hz, middle: 7-9 Hz and bottom: 11-13 Hz) for each mPFC channel was calculated, averaged per session and plotted. Increased coherence was observed at the stimulation frequency in response to stimulation (4 Hz: $p = 0.059$, $Z = -2.4$, Wilcoxon Signed Rank Test; 8 Hz: $p < .01$, $Z = -3.6$, Wilcoxon Signed Rank Test; 12 Hz: $p < .01$, $Z = -4.6$, Wilcoxon Signed Rank Test), whereas coherence of endogenous ~4-5 Hz oscillations remained unaltered in response to 8 Hz and 12 Hz stimulation (8 Hz: $p = 0.28$, $Z = 1.5$, Wilcoxon Signed Rank Test; 12 Hz: $p = 0.73$, $Z = 0.3$, Wilcoxon Signed Rank Test). Theta coherence in the 7-9 Hz band decreased upon 4 Hz or 12 Hz stimulation (4 Hz: $p = 0.01$, $Z = 3.1$, Wilcoxon Signed Rank Test; 12 Hz: $p = 0.02$, $Z = 2.9$, Wilcoxon Signed Rank Test) **C and D**. Same as **A** and **B** but for control animals. When 12 Hz stimulation was turned on, an increase in mPFC-HpC coherence was observed in the 11-13 Hz band ($p < .01$, $Z = -4.5$, Wilcoxon Signed Rank Test)

a low probability (P<0.3) of being classified into either category were not classified (n=9) and hence discarded from analysis (**Fig 3S.2A, B**).

We then assessed the effects of artificially accelerated (12 Hz), decelerated (4 Hz), or locked (8 Hz) theta oscillations on the spatial firing properties of putative principal cells in the mPFC and compared these effects with baseline firing properties during no stimulation. We confirmed that firing rates of the mPFC principal neurons remained

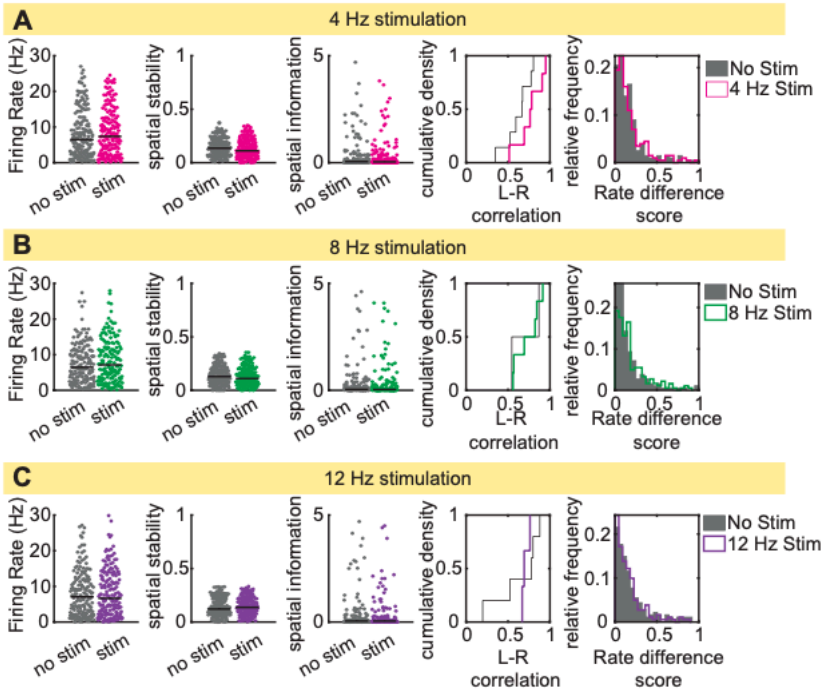

Figure 3.6 – Spatial firing properties of mPFC principal neurons remained unaltered in response to 4, 8 and 12 Hz septal stimulation.

Firing rates, spatial stability, spatial information score, L-R correlations, and rate difference scores are shown for no stimulation and stimulation blocks for all three stimulation frequencies (**A**: 4 Hz, **B**: 8 Hz, **C**: 12 Hz). Spatial firing properties remained unaltered by stimulation at any frequency compared to no stimulation.

unaltered due to stimulation (**Fig 3.6**; 4 Hz: n=178, p=0.42, Z=-0.80, 8 Hz: n=170, p=0.35, Z=-0.93, 12 Hz: n=173, p=0.96, Z=-0.04 Wilcoxon Rank Sum test). Linearized rate maps

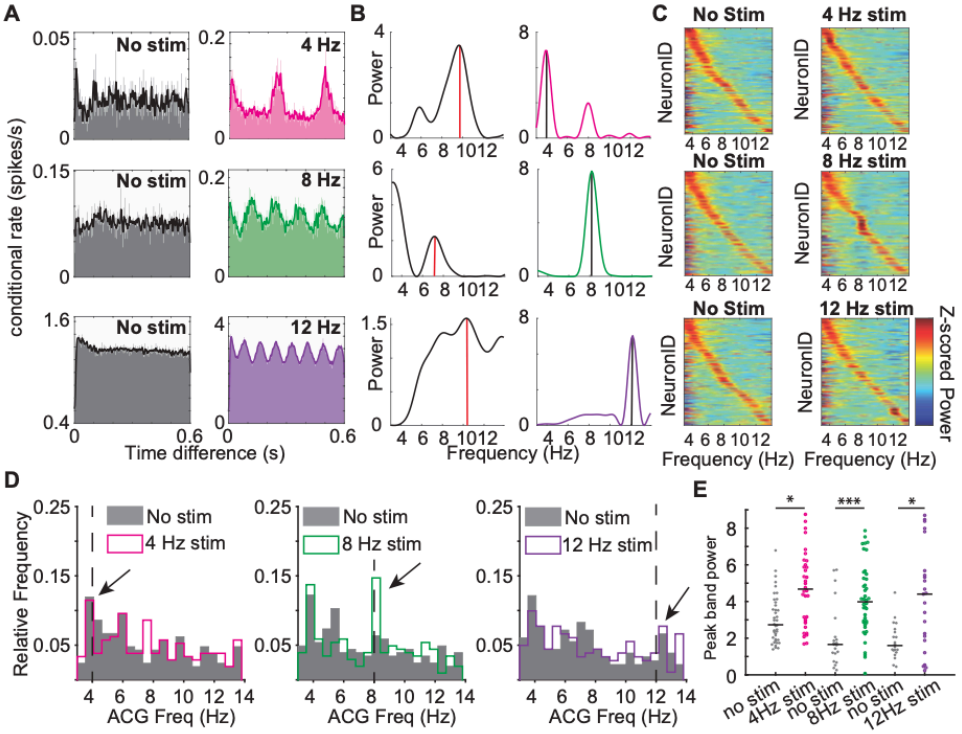

Figure 3.7 – mPFC principal cells were more strongly paced by 8 Hz septal stimulation than by 4 or 12 Hz.

A. Autocorrelogram spectra of three example neurons during no stim and stim blocks are shown (top: 4 Hz, middle: 8 Hz and bottom: 12 Hz). **B**. Autocorrelogram spectra of all mPFC principal neurons recorded from ChR2 animals sorted according to ascending order of frequency within each condition. **C**. Histograms of the peak frequencies computed from the autocorrelogram spectra during no stimulation (grey) and stimulation (4 Hz: pink, 8 Hz: green, 12 Hz: purple) conditions. Distributions of frequencies did not vary significantly between no stimulation and stimulation conditions for 4 Hz and 12 Hz stimulation frequencies, although a subset of principal cells were paced at 4 and 12 Hz. A significant subset of neurons was paced at 8 Hz in response to 8 Hz stimulation. **D**. Peak band power computed at the peak frequencies for neurons that are paced at the stimulation frequency (for example, peak frequency of 4 Hz during no stimulation versus peak frequency of 4 Hz during 4 Hz stimulation) is shown for all three stimulation frequencies. Amplitude of rhythmicity (measured by peak band power) was increased upon stimulation compared to no stimulation periods.

were computed for each neuron and were used to characterize their spatial firing. Spatial firing patterns were examined using the following measurements: (1) spatial stability, which is an indication of the consistency of firing in spatial bins across trials, (2) spatial

information score (Skaggs et al., 1996), which denotes the information in bits/spike, (3) L-R correlation, which is the correlation between firing patterns on the left and the right trajectories and (4) Rate difference score, which is calculated as the difference of maximum firing rate during the left and right trajectories divided by their sum. A higher rate difference score indicates that the firing rates between the two trajectories are more distinct. Only neurons that had a higher spatial information score compared to a shuffled distribution (>95th percentile) in either the no stimulation or the stimulation condition were considered for analysis. All four measures remained unaltered at stimulation of any frequency (**Fig 3.6** Spatial stability – 4 Hz: n=178, p= 0.30, Z=1.02, 8 Hz: n=170, p=0.23, Z=1.18, 12 Hz: n=173, p=0.35, Z=-0.92 Wilcoxon Rank Sum test; Spatial information – 4 Hz: n=178, p=0.25, Z=1.15, 8 Hz: n=170, p=0.30, Z=1.04, 12 Hz: n=173, p=0.91, Z=0.01 Wilcoxon Rank Sum test; L-R correlation – 4 Hz: n=178, p= 0.55, K Statistic=0.43, 8 Hz: n=170, p= 0.36, K Statistic=0.80, 12 Hz: n=173, p= 0.61, K Statistic=0.50 KS Test; Rate difference score – 4 Hz: n=178, p= 0.93, K Statistic=0.05, 8 Hz: n=170, p= 0.11, K Statistic=0.15, 12 Hz: n=173, p= 0.93, K Statistic=0.06 KS Test).

Artificial control of theta oscillations at stimulation frequencies has mixed effects on rhythmicity of cell firing

To assess the temporal firing properties, and specifically the rhythmicity of firing of single units, we computed autocorrelogram functions for each single unit and calculated the frequency and amplitude of the autocorrelogram spectrum. Principal cells in the mPFC were not significantly rhythmically modulated during no stimulation conditions, as

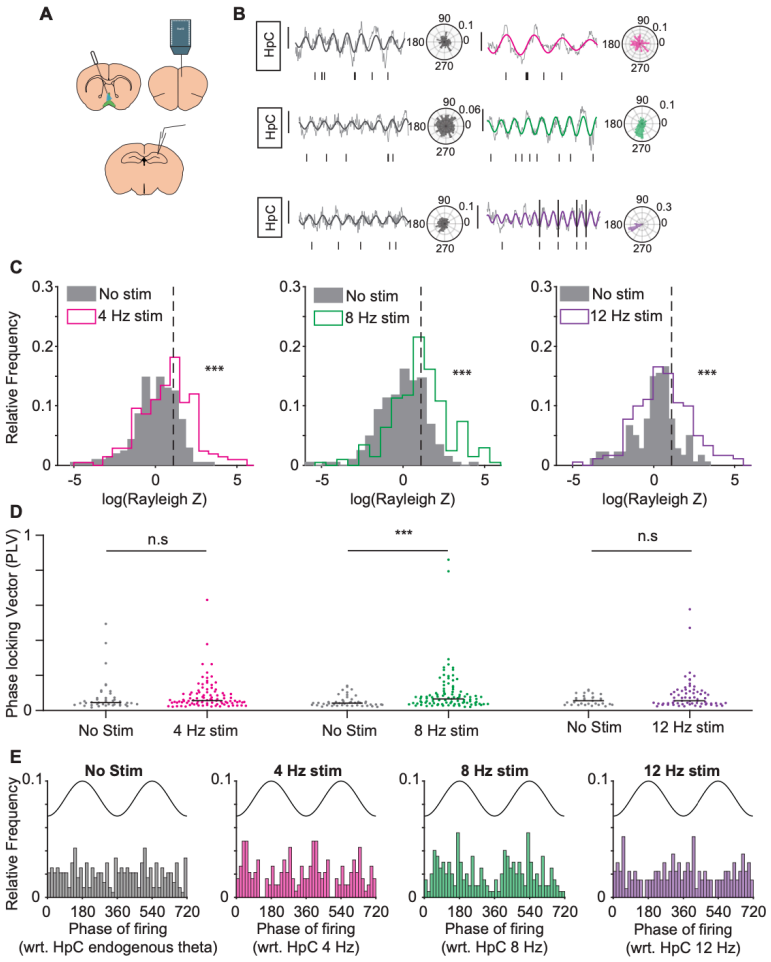

Figure 3.8 – mPFC principal cells were more strongly entrained to artificially generated oscillations at 8 Hz, but not 4 Hz or 12 Hz.

A. Recording Schematic. **B.** Example raw traces (grey) and filtered traces (thick black or colored) during stimulation and no stimulation. Ticks indicate the spike times of three example neurons recorded along with the corresponding LFP. **C**. Histograms of the distribution of log(Rayleigh Z) values are shown for no stimulation and stimulation conditions for all three stimulation frequencies (no stimulation: grey, 4 Hz: pink, 8 Hz: green, 12 Hz: purple). The dotted line indicates a significance level of p = 0.05 (Rayleigh Z test). Colored histograms show a rightward shift, with a significantly higher proportion of neurons significantly phase locked to HpC oscillations at the stimulation frequency. **D**. Phase locking value (PLV) of significantly phase locked principal neurons was significantly higher during 8 Hz and 12 Hz stimulation, but not during 4 Hz stimulation, compared to no stimulation conditions. **E**. Preferred phase of firing of significantly phase locked principal cells with respect to endogenous theta oscillations (during no stim), 4 Hz oscillation (during 4 Hz stim), 8 Hz oscillation (during 8 Hz stim), 12 Hz oscillation (during 12 Hz stim) are shown.

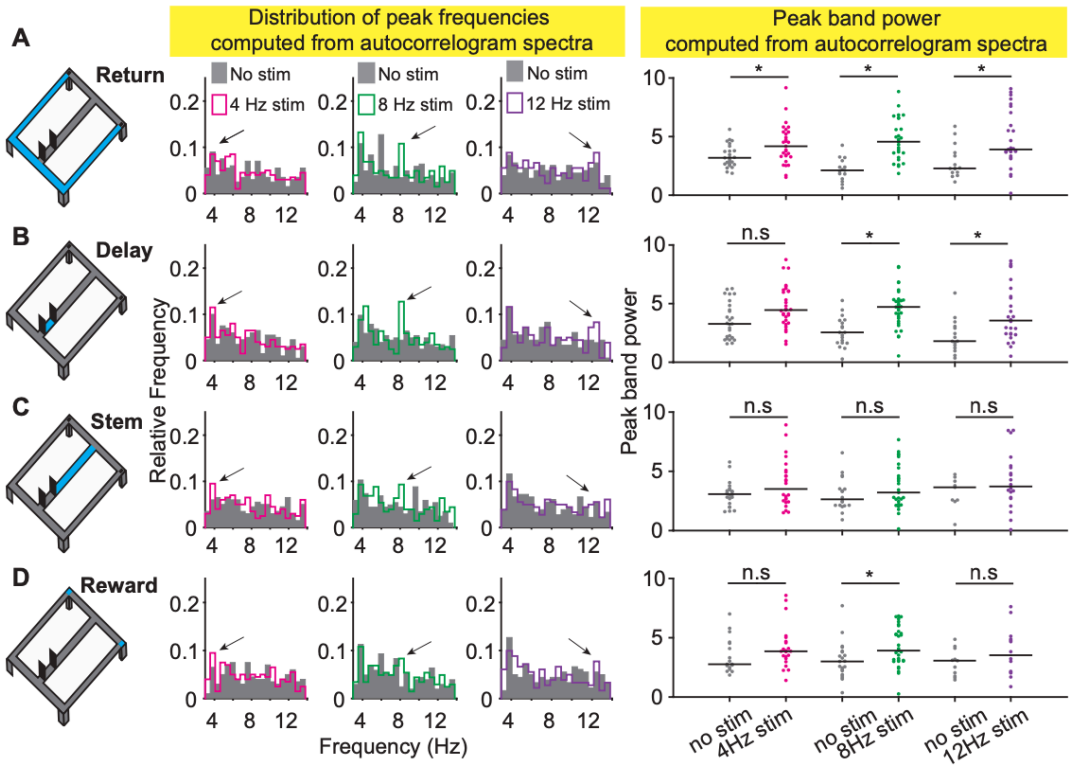

Figure 3.9 – mPFC principal cells responded strongly to optical pacing of MSA only in the return and delay zones of the maze.

A. (Left) Histograms of the peak frequencies computed from the autocorrelogram spectra during no stimulation (grey) and stimulation (4 Hz: pink, 8 Hz: green, 12 Hz: purple) conditions calculated during periods when the animal was in the return zone. (Right) Peak band power computed at the peak frequencies for neurons that are paced at the stimulation frequency (for example, peak frequency of 4 Hz during no stimulation versus peak frequency of 4 Hz during 4 Hz stimulation) is shown for all three stimulation frequencies calculated during periods when the animal was in the return zone. **B, C and D**. Same as **A** but for delay zone (**B**), stem zone (**C**) and reward zone (**D**).

indicated by the uniform distribution of peak frequencies in the 3-14 Hz range and a low peak power (**Fig 3.7A, B, D**). On the other hand, mPFC interneurons were more rhythmic at baseline compared to mPFC principal cells (**Fig 3S.3C**). Upon stimulation, a small

subset of principal cells was paced at the stimulation frequencies (**Fig 3.7C, D**). However, a larger fraction of cells was paced at 8 Hz in response to 8 Hz stimulation compared to at 4 Hz in response to 4Hz stimulation or at 12 Hz in response to 12 Hz stimulation (**Fig 3.7D**). The amplitude of pacing as measured by the peak band power was higher for all cells paced at the stimulation frequency (4 Hz, 8 Hz or 12 Hz) in response to stimulation than those that were paced at the same frequencies during no stimulation (**Fig 3.7E,** 4 Hz: $p<.05$, $Z=2.56$; 8 Hz: $p<.001$, $Z=-3.50$; 12 Hz: $p<.05$, $Z=-2.24$ Wilcoxon Rank Sum Test). Interneurons in the mPFC responded to stimulation in a similar manner as mPFC principal cells (**Fig 3S.3**), although the low interneuron numbers recorded precluded that detailed statistical analysis could be performed. We confirmed that in control animals, these effects were not observed (**Fig 3S.5A, B, C**)

Artificial theta oscillations at 4 Hz, 8 Hz and 12 Hz caused a higher proportion of mPFC principal cells and interneurons to get phase locked than during endogenous theta oscillations

To further evaluate the temporal firing characteristics of single units, we calculated the phase locking of mPFC principal cells and interneurons to endogenous and artificially paced theta oscillations in the HpC. For each single unit, we calculated the phase locking value (PLV) and preferred phase of firing with respect to the hippocampal theta oscillation (endogenous 7-9 Hz for no stimulation blocks, and stimulation frequency ±1 Hz for stimulation blocks). We also determined for each single-unit whether it was significantly phase locked with respect to the HpC oscillations. A higher proportion of principal cells

was phase locked to artificially paced theta oscillations compared to endogenous oscillations in the HpC (**Fig 3.8C** 4 Hz: p<.001, K Statistic=0.26, 8 Hz: p<.001, K Statistic=0.32, 12 Hz: p<.001, K Statistic=0.21 KS Test). We further compared the PLV of principal cells that were significantly locked to endogenous theta oscillations to that of principal cells that were significantly phase locked to artificially paced theta oscillations. Such analysis revealed that 8 Hz stimulation, but neither 4 Hz nor 12 Hz stimulation, caused an increase in the PLV (**Fig 3.8D** 4 Hz: p=0.14, Z=-1.47; 8 Hz: p<.001, Z=-3.91; 12 Hz, p=0.14, Z=-1.45 Wilcoxon Rank Sum Test). Significantly phase locked principal cells also had a preferred phase of firing during 8 Hz stimulation (**Fig 3.8E**). Phase locking of mPFC interneurons to endogenous and artificially paced HpC theta oscillations was similar to that of mPFC principal cells (**Fig 3S.4**). We confirmed that the effects were truly due to manipulation of the theta oscillations and not because of light delivery by repeating the analysis with animals in the control group (**Fig 3S.5D, E, F**).

Theta modulation of temporal firing patterns of mPFC principal cells was dependent on task phase

To investigate whether "theta" modulation of temporal firing properties of neurons within the mPFC is dependent on the task phase (for example, encoding vs maintenance vs retrieval), we parsed the maze into four zones (return, delay, stem and reward; **Fig 3.9**) and analyzed the firing patterns within each maze zone. We considered only principal cells for this analysis because we recorded a much smaller number of interneurons (n=77). Once again, only 10 s delay blocks were considered for analysis. First, we confirmed that the

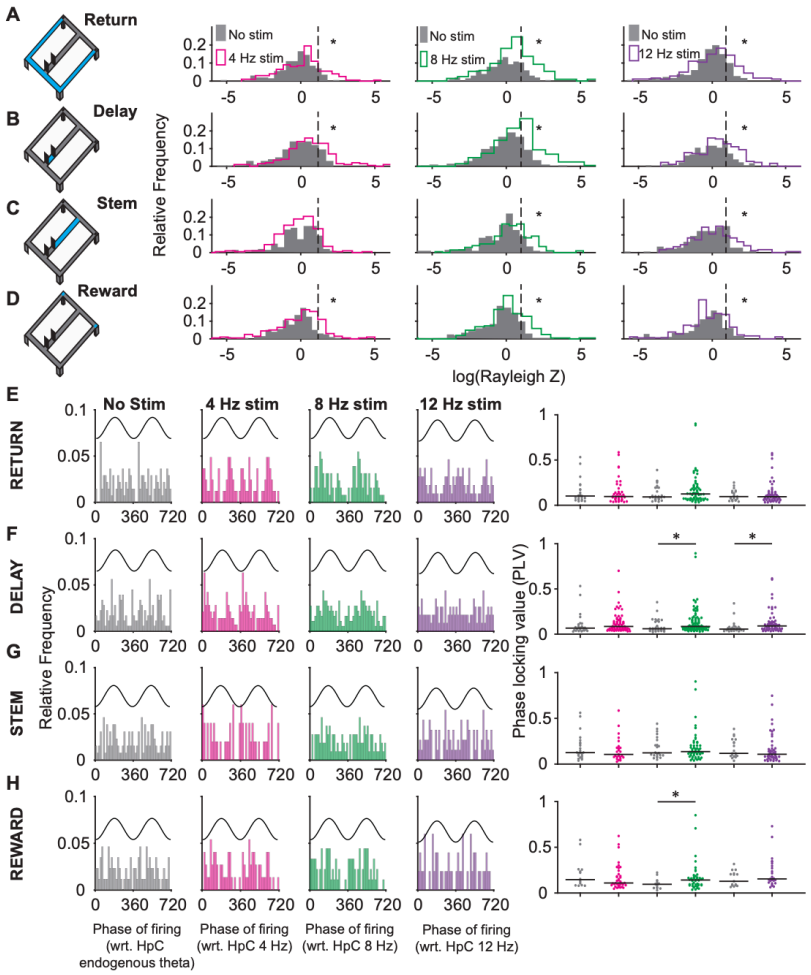

Figure 3.10 – mPFC principal cells were entrained to artificially generated oscillations only in the return and delay zones of the maze.

A. Histograms of the distribution of log(Rayleigh Z) values is shown for no stimulation and stimulation conditions for all three stim frequencies (no stim: grey, 4 Hz: pink, 8 Hz: green, 12 Hz: purple) calculated during periods when the animal was in the return zone. The dotted line indicates a significance level of p = 0.05 (Rayleigh Z test). Colored histograms show a rightward shift, with a significantly higher proportion of neurons significantly phase locked to HpC oscillations at the stimulation frequency. **B, C and D**. Same as **A** but for delay zone (**B**), stem zone (**C**) and reward zone (**D**). **E**. (Left) Preferred phase of firing of significantly phase locked principal cells with respect to endogenous theta oscillations (during no stim), 4 Hz oscillation (during 4 Hz stim), 8 Hz oscillation (during 8 Hz stim), 12 Hz oscillation (during 12 Hz stim). (Right) Phase locking value (PLV) of significantly phase locked principal neurons during 4 Hz, 8 Hz and 12 Hz stimulation calculated from periods when the animal was in the return zone. **F, G and H**. Same as **A** but for delay zone (**F**), stem zone (**G**) and reward zone (**H**).

firing rates of the mPFC principal neurons were unaffected by stimulation of any frequency in any maze zone (**Fig 3S.6B**). Then we analyzed the power spectra of the temporal autocorrelograms of the neurons on a zone-by-zone basis. The amplitude of rhythmicity was increased by 8 Hz stimulation specifically in the return, delay and reward zones and by 12 Hz stimulation only in the return and delay zones (Return – 4 Hz: $p<.05$, $Z=2.52$, 8 Hz: $p<.001$, $Z=-4.45$, 12 Hz: $p<.05$,$Z=-2.78$; Delay – 4 Hz: $p=0.07$, $Z=1.80$, 8 Hz: $p<.001$, $Z=-4.00$, 12 Hz: $p<.05$, $Z=-2.61$; Stem – 4 Hz: $p=0.16$, $Z=1.37$, 8 Hz: $p=0.26$, $Z=-1.12$, 12 Hz: $p=0.33$, $Z=-0.97$; Reward – 4 Hz: $p=0.65$, $Z=0.44$, 8 Hz: $p<.05$, $Z=-2.52$, 12 Hz: $p=0.26$, $Z=-1.12$, Wilcoxon Rank Sum Test). This suggests that mPFC principal cells responded to septally paced oscillations in a frequency dependent manner and only in the retrieval and maintenance phases of the spatial alternation task. Note that these effects were not observed in the stem zone despite running speed in the stem being similar to that in the return arm (**Fig 3S.6A, C**).

Zone-wise phase locking analysis revealed that a higher proportion of mPFC principal neurons were phase locked to artificially paced oscillations than to endogenous HpC theta oscillations in all task phases in response to all three stimulation frequencies (**Fig 3.10A**; Return – 4 Hz: $p<.01$, K statistic =0.18, 8 Hz: $p<.001$,K statistic=0.23,12 Hz: $p<.001$, K statistic =0.19; Delay – 4 Hz: $p<10^{-5}$, K statistic =0.25, 8 Hz: $p<10^{-5}$, K statistic =0.29, 12 Hz: $p<.01$, K statistic =0.18; Stem – 4 Hz: $p=0.76$, K statistic =0.04, 8 Hz: $p<.001$, K statistic =0.19, 12 Hz: $p<.05$, K statistic =0.17; Reward – 4 Hz: $p<.001$, K statistic =0.20, 8 Hz: $p<.01$, K statistic =0.18, 12 Hz: $p<.05$, K statistic =0.12, KS Test). The only exception was the 4 Hz stimulation in the stem arm, where this effect was not

observed. However, an increase in PLV was observed only in the delay zone in response to 8 Hz and 12 Hz stimulation (**Fig 3.10C;** Return – 4 Hz: p=0.91, Z=0.10, 8 Hz: p=0.46, Z=-0.73, 12 Hz: p=0.92, Z=-0.09; Delay – 4 Hz: p=0.12, Z=-1.55, 8 Hz: p<.05, Z=-2.87, 12 Hz: p<.05, Z=-2.86; Stem – 4 Hz: p=0.51, Z=0.65, 8 Hz: p=0.94, Z=-0.07, 12 Hz: p=0.33, Z=0.97; Reward – 4 Hz: p=0.39, Z= 0.85, 8 Hz: p<.05, Z=-1.97, 12 Hz: p=0.18, Z=-1.34 Wilcoxon Rank Sum Test). Our results indicate that the timing of theta oscillations mediates mPFC neuronal spiking during the encoding and the maintenance phases of the task rather than the retrieval phase.

Discussion

To better understand the mechanisms of coordination of spike timing within the mPFC and the role that theta oscillations play in this coordination, we manipulated the frequency of the oscillations and examined the responses of mPFC neurons. We first verified that our manipulation of theta oscillations paced local field potentials (LFP) within the HpC as well as the mPFC and that this manipulation was restricted to only theta oscillations and did not impact other endogenous oscillations such as the ~4-5 Hz oscillations in the mPFC. Neuronal populations within the mPFC responded to stimulation at all three frequencies, but the rhythmicity of firing as well phase locking to HpC oscillations was stronger in response to 8 Hz stimulation compared to 4 or 12 Hz stimulation. This effect was more pronounced in the return and delay zones compared to the stem and reward zones. These results augment our understanding of prefrontal-hippocampal interactions that support spatial working memory.

While septally generated LFP oscillations were coordinated between the hippocampus and the mPFC, our results indicate that a very small fraction of mPFC neurons responded to manipulations of theta oscillations. This is substantially different from the large subset of neurons in the hippocampal-entorhinal circuit that have been reported to respond to septally manipulated oscillations (Zutshi et al., 2018). Response rates are particularly high in the medial entorhinal cortex where >80% of recorded neurons respond to accelerated oscillation (10 Hz or 12 Hz) by shifting their frequency of rhythmic firing to match stimulation frequencies (Quirk et al., 2021, in press). Anatomically, the mPFC receives projections predominantly from the ventral region of the HpC (Adhikari et al., 2011). Silencing of the ventral HpC using muscimol causes a decrease in mPFC-dorsal HpC theta synchrony (O'Neill et al., 2013). While the effects of septal manipulations of theta oscillations has not been tested on oscillations in the ventral hippocampus, a key factor for reduced proportion of responsive neurons could be because of indirect projections from the MSA and the dorsal HpC to the mPFC. Alternatively, it could be that ventral hippocampal oscillations are equally well paced as dorsal hippocampal oscillations, but that projections from the ventral hippocampus to the mPFC are sparse enough so as not engage a high proportion of mPFC neurons. Furthermore, theta oscillations within the mPFC are lower in amplitude than in the dorsal hippocampus.

Our results indicate that theta modulation of prefrontal units is more pronounced in the return zone, where the previous trial trajectory might be encoded, and in the delay zone, where the encoded information is maintained until retrieval. Consistent with our results, hippocampal-prefrontal afferents have been shown to be critical during the encoding phase

of a delayed-non-match-to-place (DNMP) task (Spellman et al., 2015). On the other hand, studies that have shown prefrontal neuronal phase-locking to hippocampal theta oscillations support an effect during the retrieval of spatial memory upon learning a new task rule (Benchenane et al., 2010). Similarly, in a delayed-non-match-to-sample (DNMS) task, prefrontal neurons were phase locked to HpC theta specifically during the test or the retrieval phase of the task (Hyman et al., 2010; Hyman et al., 2005). A few key differences in these studies compared to ours could potentially explain these discrepancies. Our animals are very well trained and possibly over-trained. Moreover, our study focuses on encoding of spatial working memory in particular and not working memory in general. Mechanisms of theta-band synchrony could be drastically different in these conditions. Further, "encoding" is a term that is difficult to define in a spatial alternation task. The argument could be made that "encoding" happens during reward consumption (or non-consumption, in error trials) and that the information is merely maintained through the return and delay zones.

Interactions between the HpC and the mPFC have been shown to be mediated by theta oscillations (Backus et al., 2016; Benchenane et al., 2010; Colgin, 2011; Hyman et al., 2010; Hyman et al., 2005; Jones & Wilson, 2005; O'Neill et al., 2013; Siapas et al., 2005; Spellman et al., 2015; Zielinski et al., 2019). However, prefrontal neuronal activity has also been shown to be influenced by other brain rhythms in similar frequency ranges such as the respiration oscillation (Biskamp et al., 2017; Moberly et al., 2018; Tort et al., 2018), a 4Hz VTA mediated oscillation (Fujisawa & Buzsáki, 2011), and a 2-5 Hz rhythm mediated by the nRE (Roy et al., 2017). We demonstrated that mPFC neurons respond

more strongly to septally paced oscillations in the return and delay zones compared to other task phases, in particular with 8 Hz stimulation. Our study, thus, offers evidence that theta mediation of mPFC neuronal activity plays a crucial role in supporting spatial working memory and that this mediation occurs during the encoding phase of the task. Our results do not preclude the possibility that the mediation of prefrontal-hippocampal interactions dynamically switches from theta oscillations to other slow oscillations during the other task phases.

Materials and methods

Subjects

Thirteen mice (PV-cre 129P2-*Pvalb*$^{tm1(cre)Arbr}$/J, Jackson Labs; n = 6 male, n = 7 female) of age 2-4 months, weighing between 20-30 grams were used as subjects. All mice were housed in a reverse 12 hr dark/light cycle (lights off at 8 am). Mice were restricted to 85-90% of their *ad libitum* weight and given full access to water. All the training and testing were conducted during the dark phase. All procedures were conducted in accordance with the University of California, San Diego Institutional Animal Care and Use Committee.

Viral Injection

Six mice (3M, 3F) were injected with a viral vector expressing channelrhodospsin (ChR2; AAV.EF1α.DIO.ChR2.eGFP) and 7 mice (3M, 4F) were injected with a viral vector expressing only a fluorophore (AAV.EF1α.DIO.eGFP). Injections were targeted at

the MSA and were performed as follows. Mice were anesthetized with isoflurane (induction: 3%, maintenance: 1.5-2%) and mounted in a stereotaxic frame (David Kopf Instruments, Model 1900). The scalp was cleaned and retracted using a midline incision and the skull was leveled between bregma and lambda. A small craniotomy was made over the MSA (+1.0mm A/P, -0.7mm M/L). Injections were performed at a medio-lateral angle of 10°. A volume of 1000 nl of virus was injected at two depths (500 nl at -4.8mm D/V; 500 nl at -4.2mm D/V) at a rate of 100 nl/min using a glass pipette. The pipette was left in place for 10 minutes after each injection and retracted slowly. The incision was sutured, and the mice were allowed to recover for 5 days.

Implantation Surgery

After behavioral training, mice which met the performance criterion were selected for implantation. Mice were anesthetized with isoflurane (induction: 3%, maintenance: 1.5-2%) and mounted in a stereotaxic frame (David Kopf Instruments, Model 1900). The scalp was cleaned and retracted using a midline incision. The skull between the bregma and lambda was then leveled. Five holes were drilled in the skull to attach anchor screws. An additional hole was drilled above the cerebellum to place a ground screw. Craniotomies were performed over three brain regions (mPFC: +2.0-2.6mm A/P, 0.4mm M/L; dHpC: -1.9mm A/P, 2.0mm M/L; MSA: +1.0mm A/P, -0.7mm M/L) and dura was removed. A 32-channel silicon probe (Buzsaki32, Neuronexus) mounted on a metallic nanodrive (Cambridge Neurotech) was implanted in the mPFC region (mPFC: -0.6mm D/V) with the 4 shanks spanning anterior to posterior directions to record local field potentials and single

neuronal activity. A wire was implanted in the dHC region (dHC: -1.8mm D/V) to record local field potentials. An optic fiber was placed aimed at the MSA region at an medio-lateral angle of 10° (MSA: -3.7mm D/V) such that the fiber would lie close to the midline right above the MSA. The implant was secured with Metabond and dental cement. Postoperative care was administered as needed and mice were allowed to recover for a minimum of 5 days.

Histological Procedures

At the conclusion of the recording experiments, mice were perfused with 0.1 M phosphate-buffered saline (PBS) followed by 4% paraformaldehyde in PBS solution. Brains were post-fixed for 24 hours in 4% paraformaldehyde and then cryoprotected in 30% sucrose solution for 2 days. Brains were then frozen and sliced into 40 μm coronal sections on a sliding microtome. Sections were mounted on electrostatic slides, and stained with Fluoroshield DAPI (Sigma-Aldrich) to visualize recording locations. Slides were imaged using a virtual slide microscope (Olympus, VS120). All medial prefrontal cortex recordings were histologically confirmed to have been taken from the right infralimbic and prelimbic areas. All hippocampal recordings were histologically confirmed to have been taken from the right CA1 area.

Behavior

Mice were trained on a delayed spatial alternation task. The room was dimly lit and had stable environmental cues. The task was performed on a figure-8 maze that was 50 cm

above the ground and had dimensions of 75 cm by 50 cm. The pathway on the figure-8 maze had a width of 5 cm. The first 25 cm of the stem arm was designated as the delay zone with the help of cardboard barriers. The maze was cleaned with 70% alcohol after each animal used the maze. Animals were trained in phases. On the first day, animals were allowed to freely explore the maze for 10 minutes to habituate them. After habituation for one day, animals started the first phase of training. In the first phase, animals were forced to make the correct turns using carboard barriers. This phase lasted for 5 days. They were then rewarded with a single chocolate sprinkle (Betty Crocker Parlor Perfect Chocolate Sprinkles) at the reward zone. Care was taken to place the chocolate sprinkle at the reward location only after the animal made its choice. Animals performed 60 trials per day. After the forced-choice phase, animals were trained on the continuous version of the alternation task until they reached a criterion of >80% correct on 2 out of 3 consecutive days. Then delays (2 s and 10 s) were introduced wherein animals were forced to wait in the delay zone for the designated time. This phase of training consisted of 6 blocks of 10 trials each. Each block was designated as a 0 s, 2 s or 10 s block, and each delay condition was repeated twice. Once the animals reached a criterion of >80% correct on 2 out of 3 consecutive days, an implantation surgery was performed (see above). After at least 5 days of recovery, animals were re-trained on the delayed version of the task. Once criterion (>80% correct on 2 out of 3 consecutive days) was reached, recording and optogenetic stimulation was started. In this phase, animals performed 60 trials per day and responses on all 60 trials were recorded and analyzed.

Optogenetic stimulation

Blue light pulses (wavelength 473 nm) were delivered to a custom-made optic fiber implant targeted at the MSA using a LASER through an optic fiber patch cord (Doric Lenses, MFP_200/240/1100-0.22_10m_FC-ZF1.25(F), 200 µm core, 0.22 NA). The custom fiber optic implant was made using an optic fiber (200 µm core, Thor Labs, 0.50 NA multimode fiber) that was glued to a zirconia ferrule (Precision Fiber Products, 230 µm). The final optic fiber was sanded down to allow maximum light through the fiber and cut to a length of 4 mm. Control of the LASER system was achieved using custom written software on Arduino MEGA (ATMEGA 2560), which provided TTL pulses to the LASER system through a BNC cable. Stimulation was turned on during every alternating blocks of trials.

Electrophysiological recordings

Local Field Potentials (LFP) were recorded using chronically implanted wires. Implanted wires were threaded through a head-mounted preamplifier and connected via a tether to a 32-channel digital data acquisition system (Neuralynx, Bozeman, MT). Continuous LFP was sampled at 32000 Hz and band-pass filtered between 0.1 and 1000 Hz. Position data of a red and a green LED located on either side of the head-mounted preamplifier were tracked by a video camera at a sampling frequency of 30 Hz to determine the spatial location of the animals while they performed the task.

Pacing Scores

Pacing scores were calculated only for the continuous alternation blocks (0 s delay) within a session. Note that the animals are nearly continuously running during these blocks except during reward consumption and therefore, have the highest amplitude of endogenous theta oscillations. Because paced oscillations compete with endogenous oscillations, calculation of pacing scores with LFP recorded during 0 s delay blocks provide the most conservative estimate of pacing efficiency for the session.

LFP was downsampled to 500 Hz and time-frequency spectrograms [mtspectrumc() function in the Chronux toolbox] were calculated for the 0 s delay blocks during stimulation on and stimulation off trials. Peak frequencies were calculated for each 2-s moving window and a histogram of these peak frequencies was computed. A cluster around the stimulation frequency indicated that the LFP was artificially paced at that frequency. The maximum value of the distribution around the stimulation frequency (3-5 Hz for 4Hz stimulation, 7-9 Hz for 8Hz stimulation and 11-13 Hz for 12 Hz stimulation) was taken to be the pacing score for the session.

LFP Analysis

Raw LFP signals were down-sampled to 2000 Hz and a Morlet wavelet of width ratio = 6 was used to determine the power and phase of the oscillations at 30 log-spaced frequencies in the 3-20 Hz range. An average spectrogram was constructed for each maze zone in each trial. For each frequency, phase differences between pairs of oscillations was calculated, and coherence in each maze zone was computed as the length of the resultant

vector of phase differences in that zone.

Spike sorting

Continuous neural signals recorded at a sampling rate of 32000 Hz were passed through the Kilosort2.0 spike sorting algorithm. Sorted units were manually inspected with Phy where they were labelled as “good”, “multi-unit” or “noise”. Only well isolated “good” units that satisfied the following criteria were selected for analysis: (1) Morphological isolation (L-ratio < 0.6), (2) Spatial isolation (Isolation distance > 100) and (3) Temporal isolation with a clear refractory period (ISI violations, or spike rate within 1 ms < 0.6) . Further classification of these units into putative pyramidal cells and putative interneurons was performed on the basis of half-valley spike width and peak-to-trough duration. The half-valley spike width was calculated as half of the inverse of the peak frequency of the spike spectrum. The spectrum of the zero-padded spike was calculated with a 1024-point fft. A Gaussian Mixture Model (GMM) was used to cluster units into wide-spiking (putative principle cells) and narrow-spiking neurons (putative interneurons). Units with a low probability (P<0.3) of classification into either category were unclassified.

Spatial firing properties

Linearized rate maps were computed for each trial on the figure-8 Maze as previously described (Sabariego et al., 2019). Spatial information, spatial stability, L-R correlations and rate difference scores were calculated from the linearized rate maps.

Autocorrelogram function

To assess the rhythmicity of firing, autocorrelogram functions were computed based on the spike train of each single unit. Only 10 s delay blocks were considered for analysis. Our experimental design allowed for within-session comparison of temporal firing patterns during stimulation on and stimulation off blocks. To calculate the autocorrelogram function, spikes were first binned at a sampling frequency of 500 Hz and the temporal autocorrelation was computed from the resulting vector with the help of the MATLAB function xcorr(). Then, the Chronux function mtspectrumpb() with a padding factor equal to 2, was used to calculate the power spectrum of the temporal correlation. The frequency of the single unit was taken as the frequency with the maximum band power in the 3-14 Hz range. The amplitude of rhythmicity was taken to be the maximum band power in the 3-14 Hz range.

Phase-locking analysis

To calculate the extent of phase locking of single units to the HpC or mPFC oscillations, the LFP was first filtered in a narrow range using a bandpass filter with a linear phase response (bandpass() function in MATLAB with 'ImpulseResponse' parameter set to 'fir'). For stimulation off blocks, a frequency range of 7-9 Hz was used to calculate the phase locking to endogenous theta oscillations. For stimulation on blocks, a frequency range of 3-5 Hz for 4 Hz stimulation, 7-9 Hz for 8 Hz stimulation and 11-13 Hz for 12 Hz stimulation blocks were used. A Hilbert transform was used to calculate the instantaneous phases of the filtered oscillations (MATLAB function hilbert()). The instantaneous phases

at the spike times were used to calculate the resultant phase locking value and the resultant preferred phase of firing with the help of the Circular Statistics Toolbox (circ_r() and circ_mean() functions). Significantly phase locked units were selected as those whose distribution of firing phases were significantly non-uniform as per the Rayleigh Z test ($p<0.05$; circ_rtest() function in the Circular Statistics Toolbox).

Statistics

All statistics were performed using built-in functions in MATLAB (R2019b). Non-parametric tests such as Kruskal-Wallis, Wilcoxon tests and KS tests were performed. Circular statistics (for phase locking analysis) were performed using the Circular Statistics Toolbox. Corrections for multiple tests were performed using Holm-Bonferroni method.

Code availability

Code can be accessed at https://github.com/SunandhaSrikanth.

Acknowledgements

We thank members of the Jill Leutgeb and Stefan Leutgeb labs for valuable comments and suggestions at various stages of this project. We also thank Cory Root for permission to use the Root lab microscope. This research was supported by grants from the National Institute of Health (NS102915, NS097772 and MH119179).

Competing interests

The authors declare no competing interests.

Chapter 3, in full, is material that is currently being prepared for submission for publication by Srikanth, Sunandha; Le, Dylan; Hu, Yudi; Leutgeb, Jill K.; and Leutgeb, Stefan. The dissertation author was the primary researcher of this material.

Appendix 3.1: Supplemental Figures

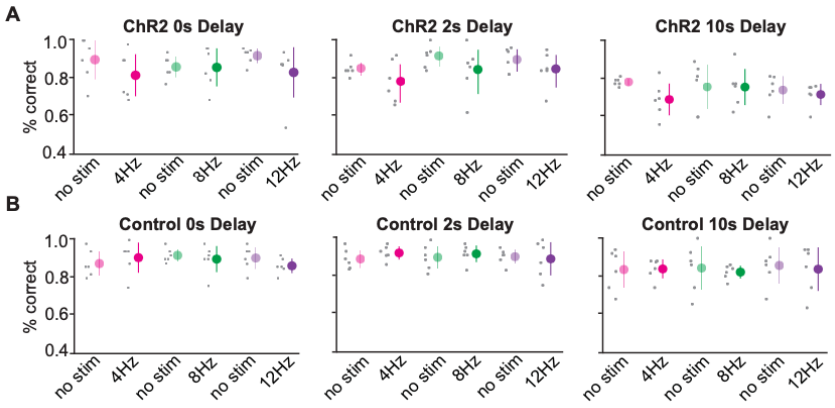

Supplemental Figure 3S.1 – Behavior results.

A and B. Behavior results (percent correct) during delay 0, delay 2, and delay 10 trials during no stim and stim blocks are shown for ChR2 animals (**A**; n=6) and control animals (**B**; n=7).

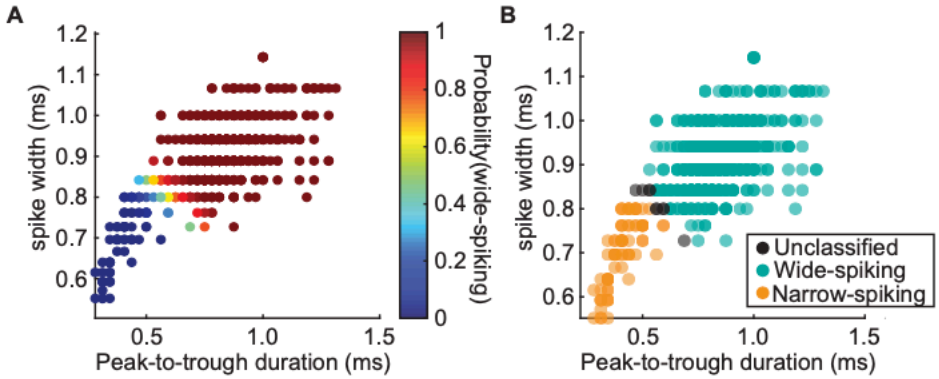

Supplemental Figure 3S.2 – Classification of mPFC neurons into wide-spiking (putative pyramidal) and narrow spiking (putative interneurons) neurons.

A. Scatter plot of spike width (ms) and peak-to-trough duration (ms) color coded by the probability of being classified as a wide-spiking neuron. A Gaussian Mixture Model (GMM) was used to determine the probability of classification. **B**. Cells with probability of classification into either class >= 0.7 were classified as wide-spiking (blue) or narrow spiking (yellow) neurons. Neurons which did not meet the criteria for classification remained unclassified and unanalyzed (black).

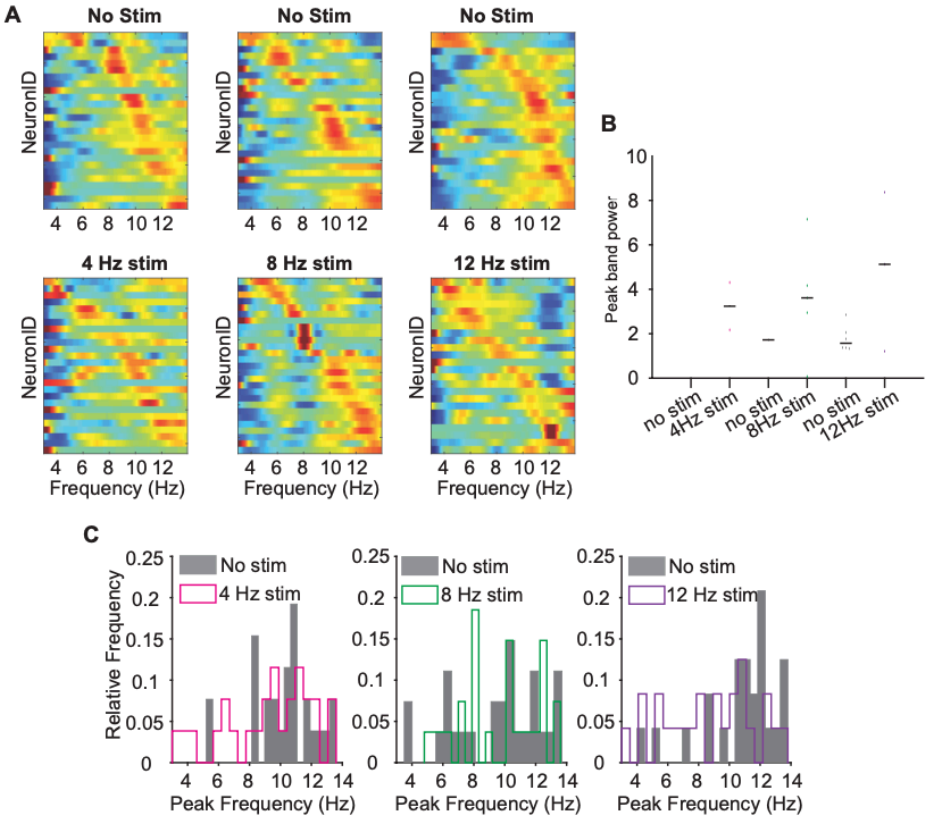

Supplemental Figure 3S.3 – mPFC interneurons were more strongly paced by 8 Hz septal stimulation than by 4 Hz or 12 Hz.

A. Autocorrelogram spectra of all mPFC interneurons recorded from ChR2 animals sorted according to ascending order of frequency within each condition. **B**. Peak band power computed at the peak frequencies for neurons that are paced at the stimulation frequency (for example, peak frequency of 4 Hz during no stimulation versus peak frequency of 4 Hz during 4 Hz stimulation) is shown for all three stimulation frequencies. Amplitude of rhythmicity (measured by peak band power) is increased upon stimulation compared to no stimulation periods but not statistically significant due to low cell numbers. **C**. Histograms of the peak frequencies computed from the autocorrelogram spectra during no stimulation (grey) and stimulation (4 Hz: pink, 8 Hz: green, 12 Hz: purple) conditions. Distributions of frequencies did not vary during no stimulation and stimulation conditions for 4 Hz and 12 Hz stimulation frequencies. A significant subset of neurons was paced at 8 Hz in response to 8 Hz stimulation (4 Hz: p=0.44, K Statistic=0.23, 8 Hz: p=0.97, K Statistic =0.13, 12 Hz: p=0.02, K Statistic =0.42 KS Test).

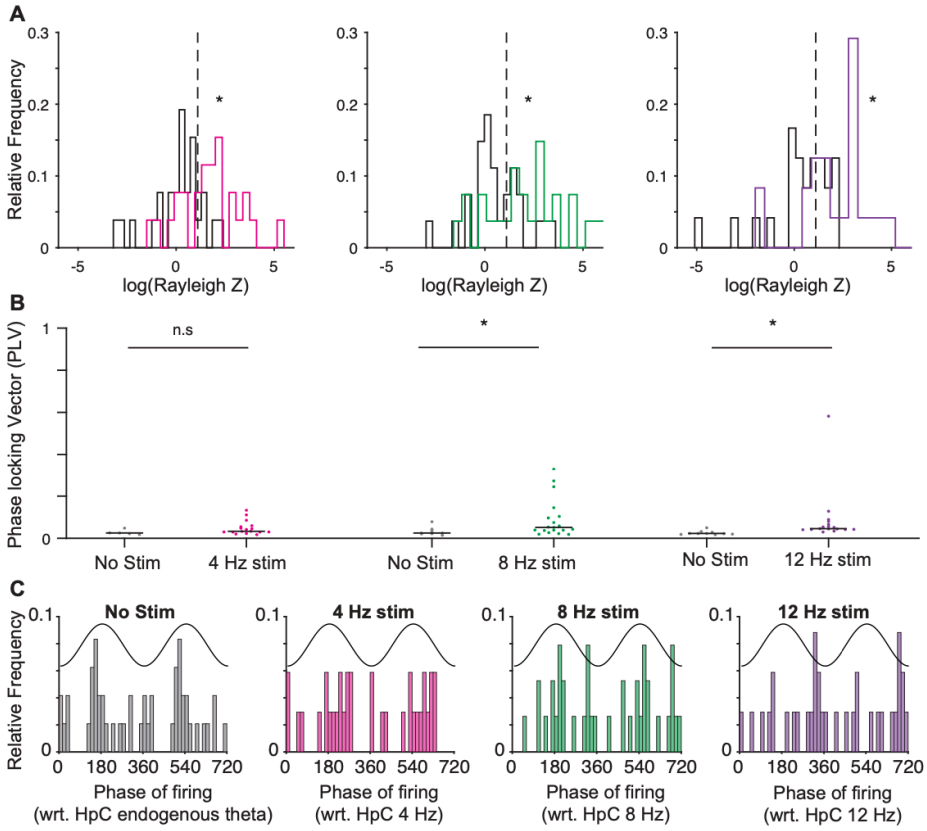

Supplemental Figure 3S.4 – mPFC interneurons were more strongly entrained to artificially generated oscillations at 8 Hz, but not 4 or 12 Hz.

A. Histograms of the distribution of log(Rayleigh Z) values is shown for no stimulation and stimulation conditions for all three stimulation frequencies (no stim: grey, 4 Hz: pink, 8 Hz: green, 12 Hz: purple). The dotted line is marked at a significance level of p = 0.05 (Rayleigh Z test). Colored histograms show a rightward shift, with a significantly higher proportion of neurons significantly phase locked to HpC oscillations at the stimulation frequency (4 Hz: p<.001, K Statistic=0.58, 8 Hz: p<.001, K Statistic =0.52, 12 Hz: p<.001, K Statistic =0.54 KS Test). **B**. Phase locking value (PLV) of significantly phase locked interneurons is significantly higher during 8 Hz and 12 Hz stimulation, but not during 4 Hz stimulation, compared to no stimulation conditions (4 Hz: p=0.09, Z=-1.65, 8Hz: p<.05, Z=-2.06, 12 Hz: p<.001, Z=-3.74 Wilcoxon Rank Sum Test). **C**. Preferred phase of firing of significantly phase locked interneurons with respect to endogenous theta oscillations (during no stim), 4 Hz oscillation (during 4 Hz stim), 8 Hz oscillation (during 8 Hz stim), 12 Hz oscillation (during 12 Hz stim).

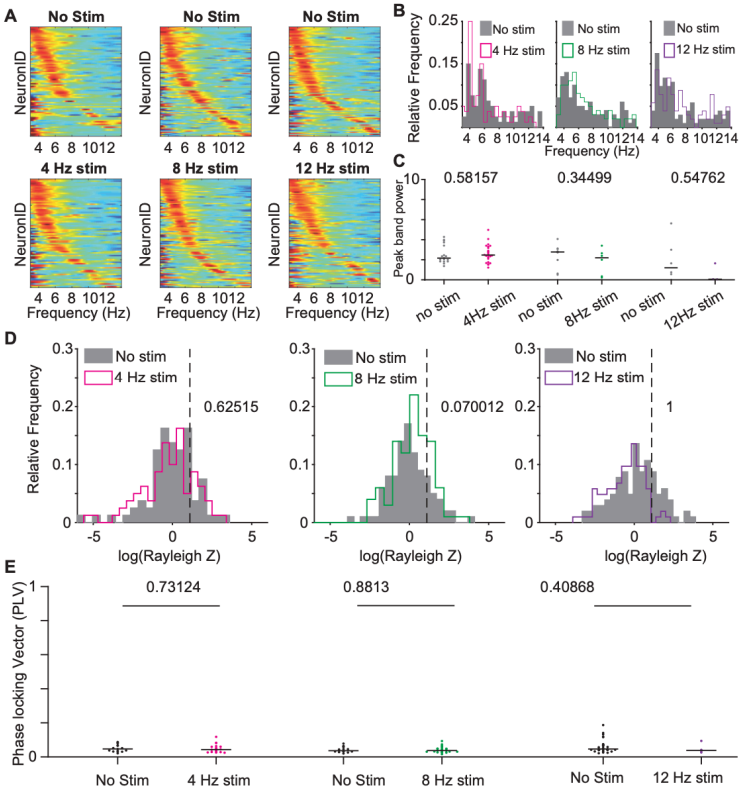

Supplemental Figure 3S.5 – mPFC principal neurons in control animals remained unresponsive to septal stimulation.

A. Autocorrelogram spectra of all mPFC principal neurons recorded from control animals sorted according to ascending order of frequency within each condition. **B**. Histograms of the peak frequencies computed from the autocorrelogram spectra during no stimulation (grey) and stimulation (4 Hz: pink, 8 Hz: green, 12 Hz: purple) conditions. Distributions of frequencies did not differ between no stimulation and stimulation conditions for any stimulation frequency (4 Hz: p=0.30, K Statistic=0.15, 8Hz: p=0.55, K Statistic=0.11, 12 Hz: p=0.31, K Statistic=0.13 KS Test). **C**. Peak band power computed at the peak frequencies for neurons that are paced at the stimulation frequency (for example, peak frequency of 4 Hz during no stimulation versus peak frequency of 4 Hz during 4 Hz stimulation) is shown for all three stimulation frequencies. Amplitude of rhythmicity (measured by peak band power) was not affected upon stimulation compared to no stimulation periods (4 Hz: p=0.58, Z=-0.55, 8Hz: p=0.34, ranksum=68, 12 Hz: p=0.54, ranksum=33 Wilcoxon Rank Sum Test). **D**. Histograms of the distribution of log(Rayleigh Z) values is shown for no stimulation and stimulation conditions for all three stimulation frequencies. No difference was observed between distributions during no stimulation and stimulation periods for any stim frequency (4 Hz: p=0.62, K Statistic=0.07, 8 Hz: p=0.07, K Statistic=0.16, 12 Hz: p=1, K Statistic=0 KS Test). **E**. Phase locking value of significantly phase locked neurons does not increase upon stimulation for any stim

frequency (4 Hz: p=0.73, Z=-0.55, 8Hz: p=0.88, Z=0.14, 12 Hz: p=0.41, Z=0.82 Wilcoxon Rank Sum Test).

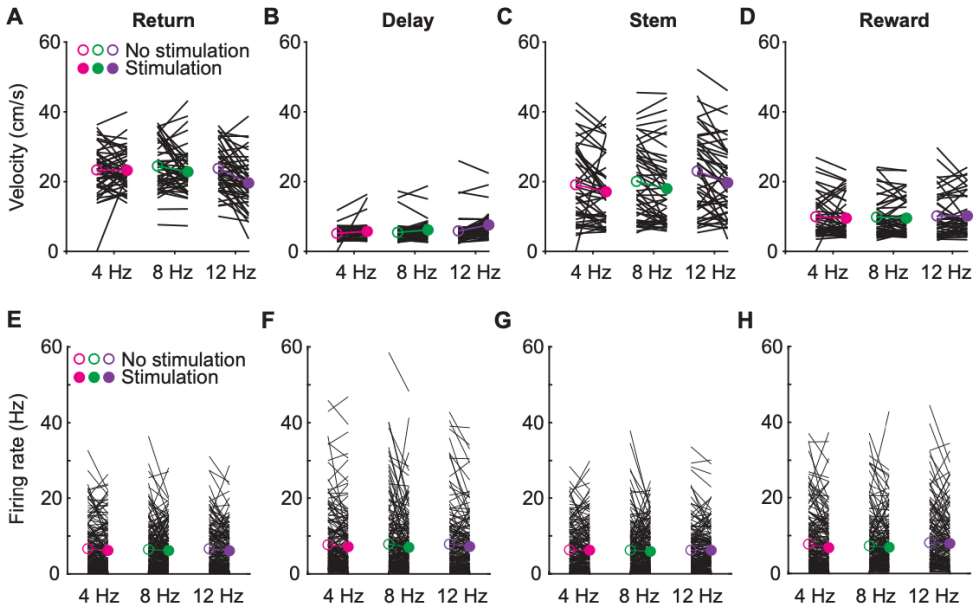

Supplemental Figure 3S.6 – Velocity and firing rates within different maze zones.

Velocity during stimulation-off (open circles) and stimulation-on (filled circles) periods within each return (**A**), delay (**B**), stem (**C**) and reward (**D**) zones in response to 4 Hz (pink), 8 Hz (green) and 12 Hz (purple) stimulation are shown. Firing rates during stimulation-off (open circles) and stimulation-on (filled circles) periods within each return (**E**), delay (**F**), stem (**G**) and reward (**H**) zones in response to 4 Hz (pink), 8 Hz (green) and 12 Hz (purple) stimulation are shown (Return – 4 Hz: p=0.06, T(199)=1.85, 8 Hz: p=0.39, T(203)=8.48, 12 Hz: p=0.07, T(180)=1.86; Delay – 4 Hz: p=0.05, T(199)=1.93, 8 Hz: p=0.06, T(203)=1.86, 12 Hz: p=0.08, T(180)=2.22; Stem – 4 Hz: p=0.73, T(199)=0.33, 8 Hz: p=0.38, T(203)=0.86, 12 Hz: p=0.87, T(180)=0.16; Reward – 4 Hz: p<.05, T(199)=3.11, 8 Hz: p=0.33, T(203)=1.04, 12 Hz: p=0.78, T(180)=0.27 Student's T-Test;). No noteworthy patterns of changes in either velocity or firing rates were observed although some comparisons were statistically significant.

REFERENCES

Adhikari, A., Topiwala, M. A., & Gordon, J. A. (2010). Synchronized activity between the ventral hippocampus and the medial prefrontal cortex during anxiety. *Neuron*, *65*(2), 257-269. https://doi.org/10.1016/j.neuron.2009.12.002

Adhikari, A., Topiwala, M. A., & Gordon, J. A. (2011). Single units in the medial prefrontal cortex with anxiety-related firing patterns are preferentially influenced by ventral hippocampal activity. *Neuron*, *71*(5), 898-910. https://doi.org/10.1016/j.neuron.2011.07.027

Adrian, E. D. (1942). Olfactory reactions in the brain of the hedgehog. *The Journal of Physiology*(459-473). https://doi.org/10.1113/jphysiol.1942.sp003955

Adrian, E. D., & Matthews, B. H. C. (1934). The Berger rhythm: potential changes from the occipital lobes in man. *Brain: A Journal of Neurology*, *57*, 355-385. https://doi.org/10.1093/brain/57.4.355

Axmacher, N., Schmitz, D. P., Weinreich, I., Elger, C. E., & Fell, J. (2008). Interaction of working memory and long-term memory in the medial temporal lobe. *Cereb Cortex*, *18*(12), 2868-2878. https://doi.org/10.1093/cercor/bhn045

Backus, A., Schoffelen, J., Szebényi, S., Hanslmayr, S., & CF, D. (2016). Hippocampal-Prefrontal Theta Oscillations Support Memory Integration. *Current biology : CB*, *26*(4). https://doi.org/10.1016/j.cub.2015.12.048

Benchenane, K., Peyrache, A., Khamassi, M., Tierney, P. L., Gioanni, Y., Battaglia, F. P., & Wiener, S. I. (2010). Coherent theta oscillations and reorganization of spike timing in the hippocampal- prefrontal network upon learning. *Neuron*, *66*(6), 921-936. https://doi.org/10.1016/j.neuron.2010.05.013

Berger, H. (1929). Über das Elektrenkephalogramm des Menschen. *Archiv für Psychiatrie und Nervenkrankheiten*, *87*(1), 527-570. https://doi.org/10.1007/BF01797193

Beshel, J., Kopell, N., & Kay, L. M. (2007). Olfactory bulb gamma oscillations are enhanced with task demands. *J Neurosci*, *27*(31), 8358-8365. https://doi.org/10.1523/JNEUROSCI.1199-07.2007

Biskamp, J., Bartos, M., & Sauer, J.-F. (2017). Organization of prefrontal network activity by respiration-related oscillations. *Scientific Reports, Published online: 28 March 2017; | doi:10.1038/srep45508*. https://doi.org/doi:10.1038/srep45508

Bland, B. H. (1986). The physiology and pharmacology of hippocampal formation theta rhythms. *Prog Neurobiol*, *26*(1), 1-54.

Bland, S. K., & Bland, B. H. (1986). Medial septal modulation of hippocampal theta cell discharges. *Brain Res*, *375*(1), 102-116.

Bramble, D., & Carrier, D. (1983). Running and breathing in mammals. *Science (New York, N.Y.)*, *219*(4582). https://doi.org/10.1126/science.6849136

Brandon, M. P., Bogaard, A. R., Libby, C. P., Connerney, M. A., Gupta, K., & Hasselmo, M. E. (2011). Reduction of theta rhythm dissociates grid cell spatial periodicity from directional tuning. *Science*, *332*(6029), 595-599. https://doi.org/10.1126/science.1201652

Buzsáki, G. (1996). The hippocampo-neocortical dialogue. *Cereb Cortex*, *6*(2), 81-92.

Buzsáki, G., & Draguhn, A. (2004). Neuronal Oscillations in Cortical Networks. https://doi.org/10.1126/science.1099745

Chapuis, J., Garcia, S., Messaoudi, B., Thevenet, M., Ferreira, G., Gervais, R., & Ravel, N. (2009). The Way an Odor Is Experienced during Aversive Conditioning Determines the Extent of the Network Recruited during Retrieval: A Multisite Electrophysiological Study in Rats. https://doi.org/10.1523/JNEUROSCI.0505-09.2009

Ciocchi, S., Passecker, J., Malagon-Vina, H., Mikus, N., & Klausberger, T. (2015). Brain computation. Selective information routing by ventral hippocampal CA1 projection neurons. *Science*, *348*(6234), 560-563. https://doi.org/10.1126/science.aaa3245

Clarke, S. (1971). Sniffing and fixed-ratio behavior for sucrose and brain stimulation reward in the rat. *Physiology & behavior*, *7*(5). https://doi.org/10.1016/0031-9384(71)90133-8

Colgin, L. L. (2011). Oscillations and hippocampal-prefrontal synchrony. *Current opinion in neurobiology*, *21*(3). https://doi.org/10.1016/j.conb.2011.04.006

Courtiol, E., Hegoburu, C., Litaudon, P., Garcia, S., Fourcaud-Trocmé, N., & Buonviso, N. (2011). Individual and synergistic effects of sniffing frequency and flow rate on olfactory bulb activity [research-article]. *https://doi.org/10.1152/jn.00672.2011*. https://doi.org/10.1152/jn.00672.2011

Dudar, J. D., Whishaw, I. Q., & Szerb, J. C. (1979). Release of acetylcholine from the hippocampus of freely moving rats during sensory stimulation and running. *Neuropharmacology*, *18*(8-9), 673-678.

Feder, R., & Ranck, J. B. (1973). Studies on single neurons in dorsal hippocampal formation and septum in unrestrained rats. II. Hippocampal slow waves and theta cell firing during bar pressing and other behaviors. *Exp Neurol*, *41*(2), 532-555.

Feldman, J. L., Del Negro, C. A., & Gray, P. A. (2013). Understanding the rhythm of breathing: so near, yet so far. *Annu Rev Physiol*, *75*, 423-452. https://doi.org/10.1146/annurev-physiol-040510-130049

Fontanini, A., Spano, P., & Bower, J. M. (2003). Ketamine-xylazine-induced slow (< 1.5 Hz) oscillations in the rat piriform (olfactory) cortex are functionally correlated with respiration. *J Neurosci*, *23*(22), 7993-8001.

Fritsch, G., & Hitzig, E. (1870). Electric excitability of the cerebrum (Uber die elektrische Erregbarkeit des Grosshirns). *Epilepsy & behavior : E&B*, *15*(2). https://doi.org/10.1016/j.yebeh.2009.03.001

Fuhrmann, F., Justus, D., Sosulina, L., Kaneko, H., Beutel, T., Friedrichs, D., Schoch, S., Schwarz, M. K., Fuhrmann, M., & Remy, S. (2015). Locomotion, Theta Oscillations, and the Speed-Correlated Firing of Hippocampal Neurons Are Controlled by a Medial Septal Glutamatergic Circuit. *Neuron*, *86*(5), 1253-1264. https://doi.org/10.1016/j.neuron.2015.05.001

Fujisawa, S., & Buzsáki, G. (2011). A 4 Hz oscillation adaptively synchronizes prefrontal, VTA, and hippocampal activities. *Neuron*, *72*(1), 153-165. https://doi.org/10.1016/j.neuron.2011.08.018

Fuster, J. M. (2009). Cortex and memory: emergence of a new paradigm. *J Cogn Neurosci*, *21*(11), 2047-2072. https://doi.org/10.1162/jocn.2009.21280

Gangadharan, G., Shin, J., Kim, S.-W., Kim, A., Paydar, A., Kim, D.-S., Miyazaki, T., Watanabe, M., Yanagawa, Y., Kim, J., Kim, Y.-S., Kim, D., & Shin, H.-S. (2016). Medial septal GABAergic projection neurons promote object exploration behavior and type 2 theta rhythm. https://doi.org/10.1073/pnas.1605019113

Gaztelu, J. M., & Buño, W. (1982). Septo-hippocampal relationships during EEG theta rhythm. *Electroencephalogr Clin Neurophysiol*, *54*(4), 375-387.

Gourévitch, B., Kay, L. M., & Martin, C. (2010). Directional coupling from the olfactory bulb to the hippocampus during a go/no-go odor discrimination task. *J Neurophysiol*, *103*(5), 2633-2641. https://doi.org/10.1152/jn.01075.2009

Headley, D. B., & Paré, D. (2017). Common oscillatory mechanisms across multiple memory systems [OriginalPaper]. *npj Science of Learning*, *2*(1), 1-8. https://doi.org/doi:10.1038/s41539-016-0001-2

Hebb, D. O. (1949). *The organization of behavior; a neuropsychological theory.* Wiley. https://doi.org/TBD

Hermer-Vazquez, R., Hermer-Vazquez, L., Srinivasan, S., & Chapin, J. K. (2007). Beta- and gamma-frequency coupling between olfactory and motor brain regions prior to skilled, olfactory-driven reaching. *Exp Brain Res*, *180*(2), 217-235. https://doi.org/10.1007/s00221-007-0850-2

Hoover, W., & Vertes, R. (2007). Anatomical analysis of afferent projections to the medial prefrontal cortex in the rat. *Brain structure & function*, *212*(2). https://doi.org/10.1007/s00429-007-0150-4

Hyman, J., Zilli, E., Paley, A., & Hasselmo, M. (2010). Working Memory Performance Correlates with Prefrontal-Hippocampal Theta Interactions but not with Prefrontal Neuron Firing Rates. *Frontiers in integrative neuroscience*, *4*. https://doi.org/10.3389/neuro.07.002.2010

Hyman, J. M., Zilli, E. A., Paley, A. M., & Hasselmo, M. E. (2005). Medial prefrontal cortex cells show dynamic modulation with the hippocampal theta rhythm dependent on behavior. *Hippocampus*, *15*(6), 739-749. https://doi.org/10.1002/hipo.20106

Hérent, C., Diem, S., Fortin, G., & Bouvier, J. (2020). Absent phasing of respiratory and locomotor rhythms in running mice. *eLife*, *9*. https://doi.org/10.7554/eLife.61919

Ito, J., Roy, S., Liu, Y., Cao, Y., Fletcher, M., Lu, L., Boughter, J. D., Grün, S., & Heck, D. H. (2014). Whisker barrel cortex delta oscillations and gamma power in the awake mouse are linked to respiration. *Nat Commun*, *5*, 3572. https://doi.org/10.1038/ncomms4572

Jessberger, J., Zhong, W., Brankačk, J., & Draguhn, A. (2016). Olfactory Bulb Field Potentials and Respiration in Sleep-Wake States of Mice [Research Article]. *Neural Plasticity*, *2016*. https://doi.org/https://doi.org/10.1155/2016/4570831

Jones, M. W., & Wilson, M. A. (2005). Theta Rhythms Coordinate Hippocampal–Prefrontal Interactions in a Spatial Memory Task. https://doi.org/10.1371/journal.pbio.0030402

Karakaş, S., & Başar, E. (2006). Models and theories of brain function in cognition within a framework of behavioral cognitive psychology. *Int J Psychophysiol*, *60*(2), 186-193. https://doi.org/10.1016/j.ijpsycho.2005.12.011

Karakaş, S., & Başar, E. (2006). Models and theories of brain function in cognition within a framework of behavioral cognitive psychology. *International journal of psychophysiology : official journal of the International Organization of Psychophysiology*, *60*(2). https://doi.org/10.1016/j.ijpsycho.2005.12.011

Kay, L. M. (2005). Theta oscillations and sensorimotor performance. *Proc Natl Acad Sci U S A*, *102*(10), 3863-3868. https://doi.org/10.1073/pnas.0407920102

Kay, L. M., & Beshel, J. (2010). A beta oscillation network in the rat olfactory system during a 2-alternative choice odor discrimination task. *J Neurophysiol*, *104*(2), 829-839. https://doi.org/10.1152/jn.00166.2010

Kay, L. M., & Freeman, W. J. (1998). Bidirectional processing in the olfactory-limbic axis during olfactory behavior. *Behav Neurosci*, *112*(3), 541-553.

Kay, L. M., & Laurent, G. (1999). Odor- and context-dependent modulation of mitral cell activity in behaving rats. *Nat Neurosci*, *2*(11), 1003-1009. https://doi.org/10.1038/14801

Kay, L. M., & Lazzara, P. (2010). How global are olfactory bulb oscillations? *J Neurophysiol*, *104*(3), 1768-1773. https://doi.org/10.1152/jn.00478.2010

Koenig, J., Linder, A. N., Leutgeb, J. K., & Leutgeb, S. (2011). The spatial periodicity of grid cells is not sustained during reduced theta oscillations. *Science*, *332*(6029), 592-595. https://doi.org/10.1126/science.1201685

Kramis, R., Vanderwolf, C. H., & Bland, B. H. (1975). Two types of hippocampal rhythmical slow activity in both the rabbit and the rat: relations to behavior and effects of atropine, diethyl ether, urethane, and pentobarbital. *Exp Neurol*, *49*(1 Pt 1), 58-85.

Kuo, T. B., Li, J. Y., Chen, C. Y., & Yang, C. C. (2011). Changes in hippocampal θ activity during initiation and maintenance of running in the rat. *Neuroscience*, *194*, 27-35. https://doi.org/10.1016/j.neuroscience.2011.08.007

Lockmann, A. L., Laplagne, D. A., Leão, R. N., & Tort, A. B. (2016). A Respiration-Coupled Rhythm in the Rat Hippocampus Independent of Theta and Slow Oscillations. *J Neurosci*, *36*(19), 5338-5352. https://doi.org/10.1523/JNEUROSCI.3452-15.2016

Macrides, F., Eichenbaum, H. B., & Forbes, W. B. (1982). Temporal relationship between sniffing and the limbic theta rhythm during odor discrimination reversal learning. *J Neurosci*, *2*(12), 1705-1717.

Martin, C., Beshel, J., & Kay, L. M. (2007). An olfacto-hippocampal network is dynamically involved in odor-discrimination learning. *J Neurophysiol*, *98*(4), 2196-2205. https://doi.org/10.1152/jn.00524.2007

Martin, C., Gervais, R., Hugues, E., Messaoudi, B., & Ravel, N. (2004). Learning modulation of odor-induced oscillatory responses in the rat olfactory bulb: a correlate of odor recognition? *J Neurosci*, *24*(2), 389-397. https://doi.org/10.1523/JNEUROSCI.3433-03.2004

Martin, C., Gervais, R., Messaoudi, B., & Ravel, N. (2006). Learning-induced oscillatory activities correlated to odour recognition: a network activity. *Eur J Neurosci*, *23*(7), 1801-1810. https://doi.org/10.1111/j.1460-9568.2006.04711.x

Mitchell, S. J., Rawlins, J. N., Steward, O., & Olton, D. S. (1982). Medial septal area lesions disrupt theta rhythm and cholinergic staining in medial entorhinal cortex and produce impaired radial arm maze behavior in rats. *J Neurosci*, *2*(3), 292-302.

Mizumori, S. J., Barnes, C. A., & McNaughton, B. L. (1989). Reversible inactivation of the medial septum: selective effects on the spontaneous unit activity of different hippocampal cell types. *Brain Res*, *500*(1-2), 99-106. https://doi.org/10.1016/0006-8993(89)90303-x

Mizumori, S. J., Perez, G. M., Alvarado, M. C., Barnes, C. A., & McNaughton, B. L. (1990). Reversible inactivation of the medial septum differentially affects two forms of learning in rats. *Brain Res*, *528*(1), 12-20. https://doi.org/10.1016/0006-8993(90)90188-h

Moberly, A. H., Schreck, M., Bhattarai, J. P., Zweifel, L. S., Luo, W., & Ma, M. (2018). Olfactory inputs modulate respiration-related rhythmic activity in the prefrontal cortex and freezing behavior. *Nat Commun*, *9*(1), 1528. https://doi.org/10.1038/s41467-018-03988-1

Morris, R. G., Garrud, P., Rawlins, J. N., & O'Keefe, J. (1982). Place navigation impaired in rats with hippocampal lesions. *Nature*, *297*(5868), 681-683. https://doi.org/10.1038/297681a0

Nguyen Chi, V., Müller, C., Wolfenstetter, T., Yanovsky, Y., Draguhn, A., Tort, A. B., & Brankačk, J. (2016). Hippocampal Respiration-Driven Rhythm Distinct from Theta Oscillations in Awake Mice. *J Neurosci*, *36*(1), 162-177. https://doi.org/10.1523/JNEUROSCI.2848-15.2016

O'Keefe, J. (1979). A review of the hippocampal place cells. *Prog Neurobiol*, *13*(4), 419-439. https://doi.org/10.1016/0301-0082(79)90005-4

O'Keefe, J., & Dostrovsky, J. (1971). The hippocampus as a spatial map. Preliminary evidence from unit activity in the freely-moving rat. *Brain Res*, *34*(1), 171-175. https://doi.org/10.1016/0006-8993(71)90358-1

O'Neill, P., Gordon, J., & Sigurdsson, T. (2013). Theta oscillations in the medial prefrontal cortex are modulated by spatial working memory and synchronize with the hippocampus through its ventral subregion. *The Journal of neuroscience : the official journal of the Society for Neuroscience*, *33*(35). https://doi.org/10.1523/JNEUROSCI.2378-13.2013

Onoda, N., & Mori, K. (1980). Depth distribution of temporal firing patterns in olfactory bulb related to air-intake cycles. *J Neurophysiol*, *44*(1), 29-39. https://doi.org/10.1152/jn.1980.44.1.29

Phillips, M. E., Sachdev, R. N., Willhite, D. C., & Shepherd, G. M. (2012). Respiration drives network activity and modulates synaptic and circuit processing of lateral inhibition in the olfactory bulb. *J Neurosci*, *32*(1), 85-98. https://doi.org/10.1523/JNEUROSCI.4278-11.2012

Reisert, J., Golden, G. J., Dibattista, M., & Gelperin, A. (2020). Dynamics of odor sampling strategies in mice. *PLoS One*, *15*(8), e0237756. https://doi.org/10.1371/journal.pone.0237756

Rojas-Líbano, D., Frederick, D. E., Egaña, J. I., & Kay, L. M. (2014). The olfactory bulb theta rhythm follows all frequencies of diaphragmatic respiration in the freely behaving rat. *Front Behav Neurosci*, *8*, 214. https://doi.org/10.3389/fnbeh.2014.00214

Rojas-Líbano, D., & Kay, L. M. (2008). Olfactory system gamma oscillations: the physiological dissection of a cognitive neural system. *Cogn Neurodyn*, *2*(3), 179-194. https://doi.org/10.1007/s11571-008-9053-1

Roy, A., Svensson, F., Mazeh, A., & Kocsis, B. (2017). Prefrontal-hippocampal coupling by theta rhythm and by 2-5 Hz oscillation in the delta band: The role of the nucleus reuniens of the thalamus. *Brain structure & function*, *222*(6). https://doi.org/10.1007/s00429-017-1374-6

Royer, S., Sirota, A., Patel, J., & Buzsáki, G. (2010). Distinct representations and theta dynamics in dorsal and ventral hippocampus. *J Neurosci*, *30*(5), 1777-1787. https://doi.org/10.1523/JNEUROSCI.4681-09.2010

Sabariego, M., Schönwald, A., Boublil, B. L., Zimmerman, D. T., Ahmadi, S., Gonzalez, N., Leibold, C., Clark, R. E., Leutgeb, J. K., & Leutgeb, S. (2019). Time Cells in the Hippocampus Are Neither Dependent on Medial Entorhinal Cortex Inputs nor Necessary for Spatial Working Memory. *Neuron*, *102*(6), 1235-1248.e1235. https://doi.org/10.1016/j.neuron.2019.04.005

Sainsbury, R. S., Heynen, A., & Montoya, C. P. (1987). Behavioral correlates of hippocampal type 2 theta in the rat. *Physiol Behav*, *39*(4), 513-519.

Scoville, W. B., & Milner, B. (1957). Loss of recent memory after bilateral hippocampal lesions. *J Neurol Neurosurg Psychiatry*, *20*(1), 11-21. https://doi.org/10.1136/jnnp.20.1.11

Shirvalkar, P. R., Rapp, P. R., & Shapiro, M. L. (2010). Bidirectional changes to hippocampal theta-gamma comodulation predict memory for recent spatial episodes. *Proc Natl Acad Sci U S A*, *107*(15), 7054-7059. https://doi.org/10.1073/pnas.0911184107

Siapas, A. G., Lubenov, E. V., & Wilson, M. A. (2005). Prefrontal phase locking to hippocampal theta oscillations. *Neuron*, *46*(1), 141-151. https://doi.org/10.1016/j.neuron.2005.02.028

Skaggs, W. E., McNaughton, B. L., Wilson, M. A., & Barnes, C. A. (1996). Theta phase precession in hippocampal neuronal populations and the compression of temporal sequences. *Hippocampus*, *6*(2), 149-172. https://doi.org/10.1002/(SICI)1098-1063(1996)6:2<149::AID-HIPO6>3.0.CO;2-K

Spellman, T., Rigotti, M., Ahmari, S. E., Fusi, S., Gogos, J. A., & Gordon, J. A. (2015). Hippocampal–prefrontal input supports spatial encoding in working memory [OriginalPaper]. *Nature*, *522*(7556), 309-314. https://doi.org/doi:10.1038/nature14445

Tort, A. B. L., Ponsel, S., Jessberger, J., Yanovsky, Y., Brankačk, J., & Draguhn, A. (2018). Parallel detection of theta and respiration-coupled oscillations

throughout the mouse brain. *Sci Rep*, *8*(1), 6432. https://doi.org/10.1038/s41598-018-24629-z

Vanderwolf, C. H. (1969). Hippocampal electrical activity and voluntary movement in the rat. *Electroencephalogr Clin Neurophysiol*, *26*(4), 407-418.

Vanderwolf, C. H., & Szechtman, H. (1987). Electrophysiological correlates of stereotyped sniffing in rats injected with apomorphine. *Pharmacol Biochem Behav*, *26*(2), 299-304. https://doi.org/10.1016/0091-3057(87)90122-5

Wang, Y., Romani, S., Lustig, B., Leonardo, A., & Pastalkova, E. (2015). Theta sequences are essential for internally generated hippocampal firing fields. *Nat Neurosci*, *18*(2), 282-288. https://doi.org/10.1038/nn.3904

Wesson, D. W., Donahou, T. N., Johnson, M. O., & Wachowiak, M. (2008). Sniffing behavior of mice during performance in odor-guided tasks. *Chem Senses*, *33*(7), 581-596. https://doi.org/10.1093/chemse/bjn029

Wesson, D. W., Varga-Wesson, A. G., Borkowski, A. H., & Wilson, D. A. (2011). Respiratory and sniffing behaviors throughout adulthood and aging in mice. *Behav Brain Res*, *223*(1), 99-106. https://doi.org/10.1016/j.bbr.2011.04.016

Wesson, D. W., Verhagen, J. V., & Wachowiak, M. (2009). Why Sniff Fast? The Relationship Between Sniff Frequency, Odor Discrimination, and Receptor Neuron Activation in the Rat [research-article]. *https://doi.org/10.1152/jn.90981.2008*. https://doi.org/10.1152/jn.90981.2008

Winson, J. (1978). Loss of hippocampal theta rhythm results in spatial memory deficit in the rat. https://doi.org/10.1126/science.663646

Wu, R., Liu, Y., Wang, L., Li, B., & Xu, F. (2017). Activity Patterns Elicited by Airflow in the Olfactory Bulb and Their Possible Functions. *J Neurosci*, *37*(44), 10700-10711. https://doi.org/10.1523/JNEUROSCI.2210-17.2017

Yanovsky, Y., Ciatipis, M., Draguhn, A., Tort, A. B., & Brankačk, J. (2014). Slow oscillations in the mouse hippocampus entrained by nasal respiration. *J Neurosci*, *34*(17), 5949-5964. https://doi.org/10.1523/JNEUROSCI.5287-13.2014

Yoder, R. M., & Pang, K. C. (2005). Involvement of GABAergic and cholinergic medial septal neurons in hippocampal theta rhythm. *Hippocampus*, *15*(3), 381-392. https://doi.org/10.1002/hipo.20062

Zielinski, M. C., Shin, J. D., & Jadhav, S. P. (2019). Coherent Coding of Spatial Position Mediated by Theta Oscillations in the Hippocampus and Prefrontal

Cortex. *The Journal of neuroscience : the official journal of the Society for Neuroscience*, *39*(23). https://doi.org/10.1523/JNEUROSCI.0106-19.2019

Zutshi, I., Brandon, M. P., Fu, M. L., Donegan, M. L., Leutgeb, J. K., & Leutgeb, S. (2018). Hippocampal Neural Circuits Respond to Optogenetic Pacing of Theta Frequencies by Generating Accelerated Oscillation Frequencies. *Curr Biol*, *28*(8), 1179-1188.e1173. https://doi.org/10.1016/j.cub.2018.02.061